SUPPLEMENTARY METHODS

Reagents and Solutions

Reagents for fluorescence microscopy (SNARF-5F-AM, SNARF-1 dextran, 6-methoxy-N-(3-sulfopropyl)quinolinium [SPQ], Texas Red dextran [10,000 MW], BAPTA-AM, fura-2-AM) were from ThermoFisher Scientific. Calbryte 590-AM was from AAT Bioquest. ELISA development kits were from Peprotech (GM-CSF Cat # 900-K30, IL-6 Cat # 900-K16, TNFα Cat # 900-K25, IL-1β Cat # 900-K95, IL-33 Cat #900-K398, hβD1 Cat #900-K202, hβD2 Cat #900-K172) or BD Biosciences (IL-8 Cat #555244). Pre-coated ELISAs were from Aviva Systems Biology (Muc7 Cat # OKEH01290, Muc5B Cat # OKEH02841, Muc5AC Cat # OKEH02840, lysozyme Cat # OKCD01349, lactoferrin Cat # OKEH02822) or LSBio (NPY Cat # LS-F5407). Intracellular cAMP from lysed cells was measured using Amersham Biosciences cAMP Biotrak Enzyme Immunoassay system (GE Healthcare) per the manufacturer's instructions using the non-acteylation protocol (sensitivity of 25-6400 fmol per assay well). Live cell imaging of cAMP utilized downward green cADDis (Montana Molecular [1]) in a baculovirus modified for mammalian cells (BacMam; [2]). IL-4, IL-13, and LPS were from Cell Signaling Technologies and prepared with carrier BSA as per the manufacturer's instructions. Poly(I:C), NPY, scrambled NPY, BIBO 3304, VIP, $VIP_{(6-28)}$, [D-p-Cl-Phe^{6},Leu^{17}]-VIP, were from Tocris. $T16A_{inh}$-A01, $CaCC_{inh}$-A01, $CFTR_{inh}$-172, NPPB, 4,4'-diisothiocyanato-2,2'-silbenedisulfonic acid (DIDS), carbachol (CCh) were from Cayman Chemical. Inorganic salts for buffers, TNFα, bumetanide, forskolin, 4,4'-dinitrostilbene-2,2'-disulfonic acid (DNDS), 5-(N,N-dimethyl)amiloride (DMA), *N*-phenyl-1-naphthylamine (NPN), and all other reagents were from Sigma-Aldrich, unless otherwise indicated below.

Antibodies for lysozyme (BGN/06/96I; Cat # ab36362), lactoferrin (2B8, Cat # ab10110), Na^{+}/K^{+} ATPase (EP1845Y; Cat # ab76020), Muc7 (Cat # ab55542), Muc5AC (Cat # ab3649), alpha-1-antitrypsin (Cat # ab20830), β2 adrenergic receptor (Cat # ab182136) and Glut1 (rabbit polyclonal; Cat# ab15039) were from Abcam. Mouse monoclonal antibody to Glut1 (SPM498; Cat # MS-10637)

was from Thermo. Antibodies to VIPR1 (Cat # AVR-001) and TMEM16A (Cat # ACL-011) were from Alomone Labs. Antibody to VIPR2 (Cat # PA3-114) was from Pierce. Antibody to NKCC1 (mouse monoclonal, clone T9) was from Developmental Studies Hybridoma Bank. Antibodies to CFTR were used as a cocktail (1:100 each); monoclonal clones 24-1 and M3A7 were from Novus Biologicals.

All solutions used were prepared as described [3, 4]. Krebs HCO_3^- buffer for isolated acinar cell experiments contained 125 NaCl, 5 KCl, 1.2 $MgCl_2$, 1.2 NaH_2PO_4, 11 glucose, and 25 $NaHCO_3$, gassed with 95% O_2 + 5% CO_2. Krebs HCO_3^- -free buffer contained 125 NaCl, 5 KCl, 1.2 $MgCl_2$, 1.2 $CaCl_2$, 1.2 NaH_2PO_4, 11 glucose, 20 HEPES, 20 sucrose, pH 7.4, gassed with 100% O_2. Solutions for buffering capacity measurement, SNARF calibration, and SPQ calibration were as described [3, 4] and are indicated below. Hank's balanced salt solution (HBSS) contained (in mM) 138 NaCl, 5.3 KCl, 0.4 KH_2PO_4, 0.34 $NaHPO_4$, 0.41 $MgSO_4$, 0.49 $MgCl_2$, 1.8 $CaCl_2$, 5.6 glucose, 20 mM HEPES pH 7.4. Unless indicated, all cell culture reagents were from Gibco. Bumetanide was used at 100 μM, H89 at 10 μM, BIBO 3304 at 1 μM, DNDS at 30 μM. Stocks were made at 1000x in DMSO.

Serous cell isolation and culture

Primary human nasal serous acinar cells were used to study Cl^-/fluid and HCO_3^- secretion. Studies of human turbinate submucosal gland serous cells are directly relevant to the understanding of mechanisms of CRS, particularly CF-related CRS, and turbinate gland serous cells approximate gland serous cells from the lower airway. We established that pig bronchial serous cell responses are identical to human turbinate serous cells [5, 6]. Working with human cells has important advantages over mice, as data from intact glands [7] and our own studies [3-6, 8, 9] have established important differences between mouse serous cells and those from pigs and humans.

Patients undergoing medically indicated sinonasal surgery were recruited from the Department of Otorhinolaryngology at the University of Pennsylvania with written informed consent as previously described [10-13]. Inclusion criteria were patients ≥18 years of age undergoing surgery for sinonasal disease (CRS) or other procedures (e.g., trans-nasal approaches to the skull base) where tissue was

classified as “control.” Exclusion criteria included history of systemic inheritable disease (e.g., granulomatosis with polyangiitis or systemic immunodeficiencies) with the exception of cystic fibrosis (CF). Members of vulnerable populations were not included.

Comparisons made here between non-CF and CF cell Cl^- and HCO_3^- secretion are valid, because SNARF and SPQ properties were identical between CF and non-CF cells, and both genotypes had identical resting $[Cl^-]_i$, resting pH_i, and intracellular pH_i buffering capacity (**supplementary figures S19-S20**). Moreover, non-CF and CF cells exhibited identical cAMP responses to VIP stimulation (**supplementary figure S6**).

Among non-CF patients, there was minimal patient-to-patient variability in the VIP-activated ion transport phenotype measured by cell shrinkage (**supplementary figure S21a-b**) once cells were removed from the tissue environment, as we previously described [6]. For ALI cultures of serous cells, we also observed minimal patient-to-patient variability in antimicrobial secretion in response to VIP (**supplementary figure s21c**) or IL-6 release in response to LPS (**supplementary figure S21d**). This is similar to surface epithelial cultures, where we find that once primary airway cells are removed from an inflammatory environment and expanded and cultured for 3-6 weeks in defined media, secondary disease-related phenotypes are removed and cells reflect a “healthy” baseline state, with responses overwhelmingly dictated by genetics, as previously described [10-18]. This allows disease-relevant *in vitro* manipulations (treatment with IL-13, NPY, etc.) with comparison of unmanipulated cells from the same patient as “control.” For these reasons and for logistical feasibility, some of the data points in each figure representing independent experiments used cells that originated from the same patient, as we have previously done [6, 10-14, 16, 19, 20]. An equal number of independent experiments, typically 2, was performed using cells from each patient to ensure that one patient could not skew results in any experiment, though minimal variability was observed as described above. All experiments shown utilized cells from multiple patients as indicated in the figure legends.

Isolated tissue was first placed in HBSS supplemented with 2 mm L-glutamine, MEM-vitamins MEM-amino acids, MEM non-essential amino acids, and 1% BSA. The epithelium was removed via

forceps and submucosal tissue was removed from the bone. The tissue was mechanically minced with scissors and then incubated for 90 min at room temperature in HBSS supplemented as above but with 1 mg/ml Collagenase P (Roche) and 10 µg/ml DNAse I (Roche) with gentle shaking. Remaining intact tissue pieces were separated from dispersed acini and acinar cells by gravity (3 min). Gland acini were separated from single epithelial or immune cells by a short centrifugation (30 sec, 500x g). The isolation protocol yielded acini and strings of acinar cells. Acini were further dispersed by incubation with 0.5 mg/ml collagenase P as above for 60 min. Cells were pelleted and washed with HBSS before being seeded onto glass coverslips for imaging or collagen-coated transwells.

For culturing, acinar cells were washed with and resuspended in 1:1 MEME:Ham's F12K plus 20% FBS, 1x cell culture pen/strep supplement (GIBCO), gentamycin (100 µg/ml), and amphotericin B (2.5 µg/ml) modified from [21]. Cells were seeded (~$3x10^5$ cells per cm^2) on transparent Falcon filters (#353095; 0.3 cm^2; 0.4 µm pores) coated with human placental collagen. After confluence, the media was changed to 1:1 MEME:Lonza bronchial epithelial basal media (BEBM) including insulin (5 µg/ml), transferrin (5 µg/ml), hydrocortisone (0.5 µg/ml), triiodothyronine (20 ng/ml), and retinoic acid (50 nM) derived from Lonza bronchial epithelial cell culture Singlequot supplements (not using included EGF, epinephrine, BPE, or gentamycin/amphotericin mix), with added 2 mg/ml BSA, 2% NuSerum, and 1% cell culture penicillin/streptomycin supplement (modified from [21]). Media lacking EGF combined with the plastic type of these transwell filters was previously shown to differentiate cells into a serous phenotype [21, 22]. After 5 days of confluence, TEER reached ~300 - 500 Ω•cm^2 and cells were fed with similar media except with 0.5% NuSerum on the basolateral side while the apical side was washed with PBS and exposed to air. Cells were used after 2-4 weeks at air-liquid interface. Unlike primary surface epithelial cells (isolated and cultured as described [13, 14, 19, 23]), serous cell ALIs did not exhibit motile cilia by light microscopy.

Surface epithelial cell isolation and culture

Air-liquid-interface cultures of primary ciliated and goblet cells were derived from surface epithelium of middle turbinate as described [13, 14, 19, 20]. Cells were enzymatically dissociated and grown to confluence in 50% DMEM/Ham's F-12 plus 50% bronchial epithelial basal media (BEBM, Lonza) for 7 days [14, 19, 20]. Dissociated cells were then seeded on Transwell filters (Corning) coated with type I bovine collagen, fibronectin, and bovine serum albumin. Culture medium was removed from the upper compartment after 5-7 days, and cells were fed basolaterally with differentiation medium containing 50% DMEM and 50% BEBM plus Lonza B-ALI Singlequot supplements as provided supplemented with 100 U/ml penicillin, 100 µg/ml streptomycin, and retinoic acid B-ALI inducer (added fresh for each feeding) as described [13, 14, 19, 20].

Imaging of intracellular cAMP dynamics in isolated nasal gland serous cells

Isolated acinar cells were plated for 30 min on glass coverslips pre-coated with growth factor reduced Matrigel (diluted 1:30 in MEM; 24 hours at 37 °C), followed by washing and addition of serum-free Ham's F12K (Gibco) containing cADDis expressing BacMam (Montana Molecular [1, 24]) plus 5 mM NaButyrate to enhance expression. Cells were imaged after 24 hrs incubation at 37 °C. Cells were imaged as above under CO_2/HCO_3^- conditions using a standard GFP/FITC filter set (Semrock) on a Nikon microscope (20x 0.75 Plan Apo objective) equipped with a QImaging Retiga R1 camera and XCite 110 LED illumination system. Data were acquired with Micromanager [25]. Experiments were done under ion substitution conditions (high K^+) to reduce volume changes as previously described [3-6, 9] to ensure that cADDis fluorescence changes were not artifacts of cell volume change during activation of secretion, confirmed by pilot experiments using mNeonGreen-only BacMam. For experiments with pertussis toxin (PTX), PTX was included with the BacMam virus infection reaction and included in media after removal of BacMam (~24 hours pretreatment).

Primary culture of human monocyte-derived macrophages (Mϕs)

Monocytes were isolated from healthy apheresis donors by RosetteSep™ Human Monocyte Enrichment Cocktail (Stem Cell Technologies) by the University of Pennsylvania Human Immunology Core and provided as de-identified untraceable cells. Monocytes were differentiated into macrophages (Mϕs) by 10 days of adherence culture in high glucose RPMI media containing 10% human serum. Differentiation to Mϕs was confirmed by functional expression of markers including histamine H1 receptors determined by Ca^{2+} imaging (**supplementary figure S22**) with specific antagonists as well as secretion of appropriate cytokines in response to M1 vs M2 polarization stimuli (**supplementary figure S10**). Induction of Mϕs NPY production was carried out by incubation in PMA (100 nM) or vehicle (0.1% DMSO) for 24 hrs, followed by washing to remove PMA and further incubated for 24 hours in fresh 300 µL media in a 24 well plate. This was based on previous work showing PMA increases Mϕ NPY production [26]. Phenol-red free media was used to facilitate ASL pH or height measurements.

Immunofluorescence (IF)

IF was carried out as previously described [10], with modifications outlined below. ALI cultures were fixed for 3 min in ice-cold methanol, followed by blocking in Dulbecco's phosphate buffered saline (DPBS) containing 1% bovine serum albumin (BSA), 5% normal donkey serum (NDS), 0.2% saponin, and 0.3% triton X-100 for 1 hour at 4°C. Primary antibody incubation was carried out at 4°C overnight. AlexaFluor-labeled donkey anti-mouse or rabbit secondary antibody incubation (1:1000) was carried out for 2 hours at 4°C. Transwell filters were removed from the plastic mounting ring and mounted with Fluoroshield with DAPI (Abcam). Images of ALIs were taken on an Olympus IX83 microscope (60x 1.4 NA objective) with spinning disc confocal unit (Olympus DSU). Images were analyzed using Metamorph software and/or the FIJI [27] version of ImageJ (W. Rasband, Research Services Branch, National Institute of Mental Health, Bethesda, MD). As VIPR1 and VIPR2

antibodies were both rabbit antibodies, co-staining was performed using Zenon antibody labeling kit (Thermo) per the manufacturer's instructions as described [19, 20].

SNARF-5F, SPQ, and DIC live-cell imaging of primary isolated serous cells

Isolation of primary serous acinar cells, immunofluorescence, and live cell imaging of acinar cell volume, pH_i (SNARF-5F), and Cl^- (SPQ) were carried out as described [3-6, 9]. After washing via gentle centrifugation and resuspension in HCO_3^- containing buffer, acinar cells were plated on Cell-Tak (BD Biosciences)-coated glass coverslips and allowed to adhere for 10–20 min in 5% CO_2. The isolation protocol yielded acini, single cells and strings of cells. Cells were identified based on visible morphology (size, polarized secretory granules, acinar structures) under DIC optics. The rationale and history of using changes in cell volume to track agonist-induced changes in secretory state is extensively described in [8, 28-30] and was performed as we previously described [3-6, 9].

Isolated acinar cells were loaded with SNARF-5F-acetoxymethyl ester (AM) for 15 min at room temperature in Krebs buffer containing 25 mM HCO_3^- gassed with 5% CO_2/95% O_2. For experiments in the absence of HCO_3^-, cells were plated in Krebs buffer lacking $NaHCO_3$ but containing 20 mM HEPES and gassed with 100% O_2. Solutions with 0-Na^+ had isosmotic replacement of NaCl with NMDG-Cl, NaH_2PO_4 with KH_2PO_4, and $NaHCO_3$ with NMDG-HCO_3. Solutions used were exactly as previously described [4]. Ratiometric fluorescence measurements of SNARF-5F were carried out using 550/20 excitation filter, 570 long pass dichroic, and 585/20 and 640/20 emission filters (Chroma Technologies set 79010-ET) housed in a filter wheel (Sutter). Excitation light was generated with an X-Cite 120 Boost LED (Excelitas Technologies) and emission was captured with an ORCA Flash 4.0 sCMOS camera (Hamamatsu) with 2x2 pixel binning. Imaging was performed on a Olympus IX-83 microscope with 30x 1.05 NA UPlanSApo silicone oil immersion objective for single cell measurements or 10x 0.4 NA PlanApo lens for ASL measurements with cells on transwells. Single cells were continuously perfused with 37°C solution gassed with 95% O_2/5% CO_2 or 100% O_2 as appropriate. Transwells were kept at 37°C with 5% CO_2 using a Tokai Hit stage-top incubator.

For experiments blocking the driving force for HCO_3^- and Cl^- efflux (performed as described [4]), we assumed $[HCO_3^-]_i$ = 16 mM based on mean resting pH of 7.2 and $[HCO_3^-]_o$ = 25 mM, making the Nernst equilibrium potential (E_{HCO3-}) ~60mV • log(16/25) = -12 mV. We have already demonstrated that the activation of secretion by serous cells results in efflux of KCl [3-6]. Mean resting $[Cl^-]_i$ was measured at ~65 mM in SPQ experiments, and with $[Cl^-]_o$ in the Krebs buffer used here at 135 mM, for a E_{Cl-} = -19 mV. $[K^+]_i$ was assumed to be 140 mM and $[K^+]_o$ was calculated at 5 mM (E_{K+} = -87 mV). Using the Nernst equation, we calculated that a using $[Cl^-]_o$ of 103 mM and $[K^+]_o$ of 89 mM would set $E_{Cl-} = E_{K+} = E_{HCO3-}$, reducing the driving force for efflux of cellular KCl and $KHCO_3$. This solution contained (in mM) 41 NaCl, 57 KCl, 32 KGluconate, 1.2 $MgCl_2$, 1 $CaCl_2$, 1.2 NaH_2PO_4, 11 glucose, 25 $NaHCO_3$, pH 7.4 by gassing with 95% O_2/5% CO_2 compared with control Krebs that contained (in mM) 125 NaCl, 5 KCl, 1.2 $MgCl_2$, 1.2 $CaCl_2$, 1.2 NaH_2PO_4, 11 glucose, 25 $NaHCO_3$, pH 7.4 by gassing with 95% O_2/5% CO_2.

SPQ measurement of $[Cl^-]_i$ changes were carried out exactly as described [3-6, 9, 14]. Rates of SPQ fluorescence changes were extrapolated to relative anion permeability [31]. Upon substitution of extracellular Cl^- for NO_3^-, electroneutral influx of NO_3^- and efflux of Cl^- decreases intracellular $[Cl^-]$ ($[Cl^-]_i$) and causes an increase in intracellular SPQ fluorescence. Because most Cl^- channels are nearly equally permeable to Cl^- and NO_3^-, relative changes in the rate of SPQ fluorescence increase is roughly equivalent to relative changes in Cl^- permeability. Isolated acinar cells were incubated for 2 hours in 20 mM SPQ at room temperature. Acinar cell ALIs were incubated overnight with 20 mM SPQ on the apical side. SPQ was imaged using a standard DAPI filter set (350/50 ex, 400 long pass dichroic, 460/50 em; Chroma 49000 ET) with UV illumination from a xenon arc lamp (Sutter Lamda LS). Solutions used for NO_3^- substitution were as previously described [3, 5, 6, 9, 14]. For ALI experiments, control normal $[Cl^-]_o$ apical solution contained (in mM) 138 NaCl, 5.3 KCl, 0.24 $MgCl_2$, 1.3 $CaCl_2$ (total $[Cl^-]_o$ = 147), 20 HEPES pH 7.4. Low $[Cl^-]_o$ solution contained (in mM) 138 $NaNO_3$ and 5.3 KNO_3 instead of NaCl and KCl, respectively (final $[Cl^-]_o$ = 4; ~37-fold less than normal $[Cl^-]_o$). For isolated acinar cells, control solution contained (in mM), 136.2 NaCl, 3.8 KCl, 1.2 KH2PO4, 1.2 CaCl2,

1.2 MgCl2, 11 glucose, 10 HEPES pH 7.4. Low $[Cl^-]_o$ solution contained NaCl replaced with $NaNO_3$ for a final $[Cl^-]_o$ of 8.6 mM. Single cells were continuously perfused with 37°C solution gassed with 95% O_2/5% CO_2 or 100% O_2 as appropriate. Transwell SPQ experiments were carried out at room temperature without gassing.

Cell volume was estimated by taking the cross-sectional area of the cell as imaged by differential interference contrast (DIC) to the 3/2 power (as described [3, 5, 6, 9, 30, 32, 33]). This method yields cell and small acini volume measurements faster than but indistinguishable from confocal 3D reconstructions [3]. Cell volumes are expressed as normalized volume (V) relative to initial cell volume (V_o). DIC images were acquired sequentially by computer controlled shuttering off of the fluorescence light, rotating of the DIC polarizer into position, and shuttering on transmitted light. Imaging data was collected and analyzed in Metafluor and/or FIJI [27].

Calibration of SNARF-5F and measurement of intracellular pH (pH_i) buffering capacity

Changes in SNARF 640/580 emission ratio were converted to pH_i using SNARF-loaded cells exposed to high $[K^+]_o$ solutions and the H^+/K^+ exchanger nigericin to equilibrate extracellular pH (pH_o) to pH_i exactly as described [4] using solutions buffered to pH_o 6.8, 7.2, and 7.6. SNARF-5F fluorescence varied linearly within the pH ranges observed during agonist stimulation.

Total pH_i buffering capacity (β_t) encompasses CO_2-HCO_3^- -dependent buffering capacity (β_{HCO3-}) plus intrinsic CO_2-independent intrinsic buffering capacity (β_i) from cytoplasmic macromolecules and organelles [4, 34, 35]. Assuming the pKa of CO_2-HCO_3^- is 6.1 [4, 35, 36] and assuming that highly permeant $[CO_2]_o = [CO_2]_i$ (1.2 mM in 5% CO_2 by Henry's Law), and using the Henderson-Hasselbach relationship, then $[HCO_3^-]_i = 1.2\ mM \times 10^{pH-6.1}$, and $\beta_{HCO3-} = 2.3 \times [HCO_3^-]_i$. Because $[CO_2]_i$ is constant (open buffering), β_{HCO3-} rises exponentially as pH_i increases [4].

Human serous acinar cell β_i was empirically determined using observed pH_i changes during exposure to NH_4Cl in Na^+/HCO_3^- -free solutions to inhibit pH_i regulatory mechanisms (as described; [4,

34, 35, 37]). Exposure of cells to solution containing NH_3 and NH_4^+ causes an initial alkalinization of pH_i due to entry of highly cell permeant NH_3 and resulting H^+ consumption as it is converted intracellularly to NH_4^+. After an experimental change in extracellular $[NH_3]$ ($[NH_3]_o$), the initial intracellular $[NH_4^+]_i$ can be calculated by Henderson-Hasselbach with $[NH_4^+]_i = [NH_3]_i \times 10^{9.2-pHi}$, assuming $[NH_3]_o = [NH_3]_i$ are identical and pKa = 9.2 [35]. Acinar cells were exposed to solutions containing (in mM) 0, 5, 10, and 20 mM $[NH_4Cl]_o$, which equilibrated to (in mM) 0, 0.6, 1.2, and 2.5 $[NH_3]_o$. The base solution for β_i buffering experiments was (in mM) 120-140 NDMG-Cl, 5 KCl, 1.2 $MgCl_2$, 1.2 $CaCl_2$, 1.2 KH_2PO_4, 11 glucose, 10 HEPES pH 7.4, and 0, 5, 10 or 20 NH_4Cl gassed with 100% O_2. Mean β_i was calculated as the units of acid of base equivalent required to change the pH_i by one unit around the midpoint of the pH change as described [4]. Raw data points for β_i were taken from experiments of 12 cells of each genotype (4 patients; 3 experiments per patient) and fit with an exponential decay function in Prism. The sum of the β_i and β_{HCO3-} curves was used to calculate β_t.

Measurements of ASL pH and ASL height

ASL height and pH measurement was carried out as described [10-14, 16, 19, 20, 38]. Cultures were imaged at 37°C in a Tokai Hit stage top incubator. For pH measurements, cells were incubated in serum-free phenol-red-free low glucose DMEM (Gibco) on the basolateral side and gassed with 5% CO_2, 20% O_2, 80% N_2. For "thin film" ASL pH measurements (main text) SNARF-1 dextran (~1 mg/ml) was sonicated in perfluorocarbon and 100 uL was added to the top of each culture. For longer-term HCO_3^- secretion experiments (**supplementary figure S11**), 100 uL of 1 mg/ml SNARF dextran in low buffering capacity solution was added (HBSS with 1 mM HEPES, as described [38]). ASL pH was calibrated by overlaying 1 mg/ml SNARF dextran on top of cultures in HCO_3^- conditions in solutions buffered with 20 mM HEPES at pH 6.8, 7.2, 7.6, and 7.8. SNARF 1 dextran pH changes were linear over the pH range observed here (~7-7.8).

ASL height was measured similarly and as previously described [11], but in HCO_3^- -free conditions (100% O_2 with basolateral HBSS buffered with 20 mM HEPES) using Texas red dextran (10,000 MW) as previously described [11]. When corrected for refractive index mismatch (1.52 η_{oil}/1.33 η_{water} = ~1.14), an observed change in ASL height of ~30 µm with agonist stimulation is in reality 30/1.14 = 26 µm. Treating the ALI as a cylinder, where volume = area x height, a change in ASL height of ~26 µm over 15 min equals a secretion volume of 2.6 µL/cm^2 (2.6x10^{-5} m x 1x10^{-4} m^2 = 2.6 x 10^{-9} m^3 = 2.6x10^{-6} L) or ~10 uL•cm^{-2}•hr^{-1}. Calu-3 cells were previously reported to secrete fluid at a rate of 4 or 5.4 uL•cm^{-2}•hr^{-1} when stimulated with forskolin or VIP, respectively, using a virtual gland technique [39]. The fact that measurements of primary serous cells here using the Texas red ASL technique are within an order of magnitude of measurements of Calu-3 cells using a different technique suggests the ASL height measurements made here are reasonable within the context of cellular fluid secretion capabilities.

Quantitative (q) PCR

RNA was isolated from ALI cultures as previously described [10] and qPCR was performed using a QuantStudio5 qPCR machine and TaqMan primer assays (Applied Biosystems/ThermoFisher Scientific) for human CFTR (Hs00357011_m1), lysozyme (Hs00426232_m1), lactoferrin (Hs00914334_m1), Muc5AC (Hs01365616_m1), Muc5B (Hs00861595_m1), Muc7 (Hs00379529_m1), Ano1 (Hs00216121_m1), pendrin (SLC26A4; Hs01070627_m1), alpha-1-antitrypsin (Hs00164575_m1), β-actin (Hs01060665_g1), beta-defensin 1 (DEFB1 Hs00608345), beta-defensin 2 (DEFB4; Hs00823638_m1), IL-6 (Hs00174131_m1), IL-8 (Hs00174103_m1), and IL-1β (Hs01555410_m1) and/or GAPDH (Hs02786623_g1) in separate reactions. Relative expression was calculated by means of the 2-ΔΔ Ct method. Comparison of β-actin with GAPDH was used as a control to validate suitability of GAPDH as a housekeeping gene in these cells.

Generation of Calu-3 air-liquid interface (ALI) cultures

Calu-3 bronchial epithelial cells (shown in **supplementary figures S7, S8, and part of S9**) were obtained from ATCC and cultured in T75 flasks in minimal essential medium (MEM) with Earl's salts and 1 mM L-glutamine, 10% fetal bovine serum, and 1% penicillin/streptomycin mix. Cells were lifted with 0.25% trypsin and plated on 1.1 cm^2 cell culture inserts (Greiner BioOne Thincerts, transparent, 0.4 µm pore size). Cells were grown to confluence for 5 days, followed by apical exposure to air and subsequent 3 weeks for full differentiation/polarization before use. Only ALIs with transepithelial resistances (TEERs) of >250-300 $\Omega \bullet cm^2$ were used.

Bacterial growth assays

Bacterial growth assays were carried out as previously described [23, 40]. *Pseudomonas aeruginosa* strains PAO1 (HER-1018; ATCC BAA-47) and clinical isolates of methicillin-resistant *Staphylococcus aureus* (MRSA) and *P. aeruginosa* were isolated by the Philadelphia VA Medical Center Microbiology Laboratory and grown in LB or tryptic soy broth (TSB; Gibco/Thermo Scientific), respectively.

Bacterial 1-N-phenylnaphthylamine (NPN) fluorescence assay was modified from previous descriptions [41-44]. *P. aeruginosa* were grown to an OD_{600} of 0.5 in LB, centrifuged, and resuspended at half volume of 10 mM HEPES, 5 mM glucose, 0.1 mM EDTA, pH 8. Bacteria were then aliquoted and mixed with an equal volume of diluted airway surface liquid secretions or antibiotics, and then pipetted into a plate reader containing an equal volume of 25% PBS containing 20 µM NPN (final NPN 10 µM, final OD_{600} 0.25). Samples were then incubated for 10 min and read on a Tecan 10M plate reader at 350 nm excitation and 450 nm emission. Samples were read in triplicate, with averages of ≥3 independent experiments reported.

CFU antimicrobial assays with Calu-3 ASL washings were carried out similarly to a previously published protocol [12, 45] and modified based on our own antimicrobial ASL protocols used in our lab [12, 40]. Cultures were washed copiously with PBS and transferred to antibiotic-free MEME for 48

hrs. before use. Calu-3 cell secretions were collected from 3 week old ALIs stimulated basolaterally with 100 μM isoproterenol for 72 hours, followed by washing of the apical surface with 30 μL 25% PBS. While washing a 1.1 cm^2 ALIs with 30 μL significantly dilutes the ASL fluid (~1 μL per cm^2 of surface area [46]), washings retained antibacterial activity and were thus sufficient to be used for this assay. ASL washings (30 μL per culture) were pooled and mixed with bacteria resuspended in 25% PBS, adjusted to 0.1 OD, then diluted 1:1000 in 25% PBS). Bacteria and ASL mixture was incubated statically in a 96-well plate at 37 °C for 2 hrs, followed by 4 serial 10-fold dilutions and spot plating onto LB plates. After overnight incubation at 37 °C, CFUs were manually counted.

CFU antimicrobial assays with primary serous cell ASL washings were carried out as above, but cultures were not pre-treated with isoproterenol. Cultures were unstimulated or stimulated for 30 min with VIP ± NPY ± scrambled NPY on the basolateral side. Afterward, the surface of a 0.33 cm^2 transwell was washed with 50 uL 25% saline (thus ASL was ~5x more dilute than used in Calu-3 experiments).

Live-dead staining was carried out with BacLight Live/Dead kit (ThermoFisher Scientific) consisting of Syto9 (live cell stain) and propidium iodide (dead cell stain), as previously used with *P. aeruginosa* [10]. Bacteria were adjusted to an OD = 0.1. Bacterial suspension was mixed with ASL (25 μL each) in a black microplate and incubated for indicated time at 37 °C. 50 μL 2x Live-Dead staining solution was then added, followed by further 10 min incubation at room temp and reading on a fluorescence microplate reader (Tecan Spark 10M) at 488 excitation and dual emission wavelengths as indicated. Control calibration of live dead staining was carried out by mixing heat-killed (as below) with live bacteria at the indicated ratios to a final OD of 0.1 followed by mixing with 25 % saline only and incubation as above prior to live dead staining.

Production of heat-killed bacteria

Bacteria were heat killed according to a previously published protocol [47]. *P. aeruginosa* or MRSA strains were grown overnight at 37°C in LB broth, then resuspended in LB and grown for 2-4

hours to an OD600 of 1. Bacteria were heat killed for 20 min at 95°C. Cells were treated with bacteria diluted to OD_{600} = 0.005 (200x dilution) in 100 uL PBS on the apical side only. Unstimulated control cultures were treated with 1:200 LB media only.

Western blotting of primary gland cells

Serous ALIs were washed 3x with PBS (apical and basolateral sides), then scrapped and pelleted with a pulse spin on a tabletop microfuge. Pellets were lysed using RIPA Buffer (20 mM Tris pH 7.5, 150 mM NaCl, 1% IgePal, 1% deoxycholate, 1 mM DTT, Complete protease inhibitor cocktail (Roche); 60ug of post 800xg cell lysate was separated on a 4-12% Bis-Tris NuPage SDS-PAGE gels using MOPS (Muc5B, Muc7, VIPR1, VIPR2) or MES (NKCC1, A1AT, NPY1R, NPY4R) running buffer with See-Blue Plus2 markers (Thermo). Different marker molecular weights are due to MOPS vs MES running buffers. As we found that NPY1R and NPY4R aggregated at the top of the gel when boiled (common for hydrophobic transmembrane GPCRs), we ran these samples without heating, which likely reflects why these proteins were observed as dimers (also common for GPCRs). Antibodies were used at a 1:1000 dilution followed by secondary HRP-linked antibodies and BioRad Clarity western ECL substrate.

SUPPLEMENTARY TABLE S1 Characteristics of CF (blue; n = 9) and non-CF (green; n = 42) patients from whom samples were used in this study.

Patient	Age at Surgery	Gender	Ethnicity	Primary Diagnosis	# Prior FESS	Polyps	Lund-Mackay	SNOT-22	Smoking History	Asthma	AFS	Abx	Steroids	Comorbidities	CF genotype
CF1	26	Female	Caucasian	CRS	1	No	N/A	78	No	Yes	No	No	No	CF, GERD, DM	F508del/F508del
CF2	23	Male	Caucasian	CRS	1	Yes	N/A	N/A	No	No	No	No	No	CF, GERD	F508del/F508del
CF3	33	Female	Caucasian	CRS	1	Yes	13	8	No	No	No	No	No	CF, Double Lung Transplant, Allergies, GERD, HTN, DM	F508del/F508del
CF4	32	Female	Caucasian	CRS	1	Yes	N/A	77	No	Yes	No	No	No	CF, GERD	F508del/F508del
CF5	58	Female	Caucasian	CRS	2	Yes	18	27	No	Yes	No	No	No	CF, Allergies, GERD, HTN	F508del/F508del
CF6	27	Female	Caucasian	CRS	0	No	N/A	59	No	Yes	No	No	No	CF	F508del/G542X
CF7	28	Female	Caucasian	CRS	0	Yes	12	45	No	Yes	No	No	No	CF, Allergies	F508del/F508del
CF8	38	Female	Caucasian	CRS	1	Yes	16	93	No	No	No	No	Yes	CF,, Lung transplant, DM	F508del/F508del
CF9	42	Male	Caucasian	CRS	1	No	14	33	No	Yes	No	Yes	No	CF, Lung transplant, DM, GERD, HTN	F508del/E585X
non-CF1	34	Male	Caucasian	CRS	0	Yes	N/A	N/A	No	No	No	No	No	Allergies	N/A
non-CF2	56	Female	Caucasian	CSF leak	0	No	N/A	N/A	No	No	No	No	No	Hypothyroid	N/A
non-CF3	65	Male	Caucasian	IP	0	Yes	4	N/A	No	No	No	No	Yes	N/A	N/A
non-CF4	71	Male	Caucasian	CRS	2	Yes	24	8	No	Yes	No	No	Yes	Samters triad, Hypothyroid	N/A
non-CF5	71	Male	Caucasian	CRS	4	Yes	18	13	No	No	No	No	No	Samter's triad, Allergies, GERD, AERD, OSA, HTN	N/A
non-CF6	60	Male	Caucasian	CRS	1	Yes	11	57	No	No	No	No	Yes	N/A	N/A
non-CF7	59	Female	Caucasian	CRS	0	No	N/A	61	No	No	No	No	No	DM, GERD, HTN	N/A
non-CF8	66	Male	Caucasian	CRS	0	Yes	N/A	18	No	No	No	No	Yes	N/A	N/A
non-CF9	76	Female	Caucasian	Pituitary microadenoma	0	No	N/A	N/A	No	No	No	No	No	HTN, CAD, PVD	N/A
non-CF10	60	Male	Caucasian	CRS	0	Yes	N/A	N/A	No	Yes	No	No	No	N/A	N/A
non-CF11	46	Female	Hispanic, Latino	CRS	1	Yes	N/A	95	No	Yes	No	No	Yes	Obesity	N/A
non-CF12	48	Male	Caucasian	CRS	0	No	N/A	N/A	No	No	No	No	Yes	OSA, COPD	N/A
non-CF13	56	Female	Caucasian	CRS	0	Yes	N/A	27	No	No	No	No	No	N/A	N/A
non-CF14	69	Male	Caucasian	CRS	3	Yes	N/A	12	No	No	No	No	No	N/A	N/A
non-CF15	34	Male	Caucasian	CRS	0	Yes	N/A	N/A	No	No	No	No	No	Allergies	N/A
non-CF16	56	Female	Caucasian	CSF leak	0	No	N/A	N/A	No	No	No	No	No	hypothyroid	N/A
non-CF17	65	Male	Caucasian	IP	0	Yes	4	N/A	No	No	No	No	Yes	N/A	N/A
non-CF18	71	Male	Caucasian	CRS	2	Yes	24	8	No	Yes	No	No	Yes	Samter's triad, hypothyroid	N/A
non-CF19	78	Female	African American	Control/skull base tumor	0	No	N/A	19	No	No	No	No	No	HTN, Allergies	N/A
non-CF20	19	Male	Caucasian	CRS	1	Yes	N/A	41	No	Yes	No	No	No	Allergies	N/A
non-CF21	44	Female	Caucasian	CRS	0	No	6	27	No	Yes	No	No	Yes	Pacemaker	N/A
non-CF22	70	Female	Caucasian	CRS	0	No	8	61	No	No	No	Yes	Yes	HTN	N/A
non-CF23	57	Male	Caucasian	CRS	0	Yes	15	16	No	No	No	Yes	No	Allergies	N/A
non-CF24	37	Male	Caucasian	CRS	1	Yes	18	68	Yes	No	No	No	No	Allergies, Sinonasal Trauma	N/A
non-CF25	60	Female	Caucasian	Control/skull base tumor	0	Yes	14	9	Yes	Yes	No	No	Yes	DM, HTN, OSA, IP	N/A
non-CF26	24	Female	Caucasian	CRS	0	No	13	69	No	No	No	No	No	Allergies, GERD	N/A
non-CF27	83	Male	Caucasian	CRS	1	Yes	3	10	No	No	No	No	No	HTN	N/A
non-CF28	52	Male	Caucasian	Fungal Ball	0	Yes	15	35	No	No	Yes	No	No	Allergies	N/A
non-CF29	60	Female	Caucasian	CRS	2	Yes	16	53	No	Yes	No	No	No	Samter's Triad, Allergies	N/A
non-CF30	61	Female	Caucasian	CRS	0	Yes	N/A	46	Yes	Yes	No	Yes	Yes	HTN	N/A
non-CF31	65	Male	Caucasian	CRS	1	No	N/A	52	No	Yes	No	No	Yes	HTN, GERD	N/A
non-CF32	62	Female	Native American	CRS	2	No	6	45	Yes	No	No	No	No	HTN	N/A
non-CF33	49	Male	Caucasian	CRS	1	No	14	56	No	Yes	No	No	Yes	OSA, HTN, MI, GERD	N/A
non-CF34	72	Female	Caucasian	CRS	3	No	9	49	No	Yes	Yes	No	Yes	GERD, HTN	N/A
non-CF35	51	Female	Caucasian	CRS	1	No	4	7	No	No	No	No	No	COPD, DM, OSA, GERD, Allergies	N/A
non-CF36	40	Male	Caucasian	CRS	1	No	13	27	No	No	No	No	No	Allergies	N/A
non-CF37	42	Male	Caucasian	CRS	0	No	5	68	No	No	No	No	No	HTN, OSA	N/A
non-CF38	57	Female	Caucasian	CRS	0	No	5	14	No	No	No	No	No	GERD	N/A
non-CF39	79	Male	Caucasian	CRS	0	Yes	11	22	No	No	No	No	No	Afib, CAD, HTN	N/A
non-CF40	57	Male	Caucasian	CRS	0	No	7	11	Yes	No	No	No	No	OSA	N/A
non-CF41	54	Male	Caucasian	CRS	0	No	7	78	No	No	No	No	No	GERD	N/A
non-CF42	38	Male	Caucasian	CRS	0	No	3	5	No	No	No	No	No	GERD	N/A

Abbreviations: Abx, antibiotics; AERD, asprin-exacerbated respiratory disease; AFS, allergic fungal sinusitis; CF, cystic fibrosis; COPD, chronic obstructive pulmonary disease; CRS, chronic rhinosinusitis; CSF, cerebrospinal fluid; DM, diabetes mellitus; FESS, functional endoscopic sinus surgery; GERD, gastroesophageal reflux disease; HTN, hypertension; IP, inverted papilloma; Lund-Mackay, sinonasal staging algorithm score [48, 49]; N/A, not available; OSA, obstructive sleep apnea; SNOT-22, 22 question sinonasal outcomes test [50]

SUPPLEMENTARY TABLE S2 Gene expression output from the Cancer Cell Line Encyclopedia (accessed 26 April, 2019; https://portals.broadinstitute.org/ccle [51]) for NPY receptors, VIP receptors, and serous cell markers lysozyme (LYZ) and CFTR. Note that Calu-3 cells, a bronchial adenocarcinoma line frequently used as a model of serous cells due to high CFTR and lysozyme expression, express the highest amount of NPY1R relative to other airway cancer cell lines.

Affymetrix

Gene	NPY1R	NPY2R	NPY5R	VIPR1	VIPR2	LYZ	CFTR
A549_LUNG	3.97359	3.910246	4.316899	5.347613	4.442829	3.861464	3.98063
CALU1_LUNG	4.150831	3.587063	4.239859	7.542943	4.087702	3.718109	3.854273
CALU3_LUNG	7.168295	3.803298	4.45895	6.922686	4.311346	11.0784	10.05969
CALU6_LUNG	3.512282	3.750993	4.158273	8.829339	4.305164	6.284744	4.588329
NCIH292_LUNG	3.553423	3.486564	3.898884	6.090106	4.314193	3.713948	3.729571
NCIH441_LUNG	3.701913	3.58951	4.291047	7.25233	4.440556	3.726355	4.128871
NCIH520_LUNG	3.952049	3.850606	4.148694	5.315201	4.260294	4.190855	4.465682
NCIH522_LUNG	3.666311	3.629025	4.243514	5.523483	4.433325	3.896822	3.716021

RNAseq

Gene	NPY1R	NPY2R	NPY4R	NPY5R	VIPR1	VIPR2	LYZ	CFTR
A549_LUNG	-5.3022356	-3.1772462	5.69438127	-13	-4.4839539	-8.4031139	-4.837362	-6.4493319
CALU1_LUNG	-1.6370841	-13	-0.0247348	-13	1.83239394	-13	-3.4844883	-4.3859648
CALU3_LUNG	0.76601676	-13	-2.4547363	-1.7320273	0.81640217	-13	7.36181905	6.44949113
CALU6_LUNG	-4.1292877	-7.6433373	-5.1671067	-6.7017855	3.62349708	-9.1687653	1.71665862	0.66432141
NCIH292_LUNG	-8.8698593	-13	0.67477717	-13	0.85130002	-0.6510655	-2.2350607	-7.3064622
NCIH441_LUNG	-13	-13	-4.4713423	-13	1.79193401	-6.2665501	-3.3788701	-5.7721996
NCIH520_LUNG	-4.5970396	-13	-6.0181873	-13	-3.6856484	-9.4348835	-0.494092	-3.896139
NCIH522_LUNG	-7.686093	-13	-6.7853125	-13	-3.0377362	-6.6170462	-1.6362569	-5.7076583

SUPPLEMENTARY TABLE S3 Gene expression output from MERAV database (accessed 11 July 2018; http://merav.wi.mit.edu/ [52]). Similar to the Cancer Cell Line Atlas data above, MERAV suggested Calu-3 cells expressed the highest amount of NPY1R among frequently used lung cancer cell lines.

GENE	NPY1R	NPY2R	NPY4R	NPY5R	NPY6R	VIPR1	VIPR2	LYZ	CFTR
A549 Lung_Cancer.Cell.Line_Large_A549_Non-Small.Cell.Lung.Carcinoma: METIS_p_NCLE_RNA1_Human_U133_Plus_2.0_H01_241018	20.28	19.39	104.89	29.99	64.41	69.52	54	28.38	24.6
A549 Lung_Cancer.Cell.Line_Large_A549_Non-Small.Cell.Lung.Carcinoma: GSM139646	16.49	17.66	78.19	20.19	66.14	73.3	58.19	26.4	24.02
A549 Lung_Cancer.Cell.Line_Large_A549_Non-Small.Cell.Lung.Carcinoma: GSM253203	26.74	19.48	46.55	43.68	136.8	130.62	54.08	24.67	24.66
A549 Lung_Cancer.Cell.Line_Large_A549_Non-Small.Cell.Lung.Carcinoma: GSM274739	18.43	17.99	111.42	36.73	87.56	81.09	50.29	25.34	24.33
A549 Lung_Cancer.Cell.Line_Large_A549_Non-Small.Cell.Lung.Carcinoma: GSM274740	20.94	20.97	141.78	35.76	83.06	77.51	42.31	24.14	24.59
A549 Lung_Cancer.Cell.Line_Large_A549_Non-Small.Cell.Lung.Carcinoma: GSM433024	55.74	20.57	76.52	39.55	70.34	95.51	55.45	25.13	26.5
A549 Lung_Cancer.Cell.Line_Large_A549_Non-Small.Cell.Lung.Carcinoma: GSM433025	57.1	24.58	81.78	31.01	66.64	92.39	52.3	28.06	20.06
Calu3 Lung_Cancer.Cell.Line_Large_Calu-3_Adenocarcinoma: WATCH_p_NCLE_RNA8_HG-U133_Plus_2_A02_474612	128.77	18	45.06	34.25	66.32	195.12	47.65	872.07	708.73
Calu6 Lung_Cancer.Cell.Line_Large_Calu-6_Adenocarcinoma: BRAKE_p_NCLE_RNA2_HG-U133_Plus_2_E04_241144	13.41	16.41	50.21	26.83	94.21	447.11	44.95	68.77	32.67
Calu 6 Lung_Cancer.Cell.Line_Large_Calu-6_Adenocarcinoma: Calu-6_SS474757_HG-U133_Plus_2_HCHP-225882_	17.07	15.34	32.14	40.08	73.67	564.18	45.56	105.84	26.02
Calu-6 Lung_Cancer.Cell.Line_Large_Calu-6_Adenocarcinoma: Calu-6_SS474758_HG-U133_Plus_2_HCHP-225883_	16.23	17.07	30.89	36.32	79.62	567.31	44.38	109.59	25.33
Calu-6 Lung_Cancer.Cell.Line_Large_Calu-6_Adenocarcinoma: Calu-6_SS474759_HG-U133_Plus_2_HCHP-225884_	19.51	17.4	34.71	32.74	69.48	552.72	47.16	104.84	25.04
H292 Lung_Cancer.Cell.Line_Large_NCI-H292_Mucoepidermoid.Carcinoma: GSM274745	15.82	14.98	44.11	39.69	75.71	116.55	48.99	27.7	21.59
H292 Lung_Cancer.Cell.Line_Large_NCI-H292_Mucoepidermoid.Carcinoma: GSM274746	15.69	16.33	47.04	34.49	74.92	89.52	50.44	24.76	22.58
H441 Lung_Cancer.Cell.Line_Large_NCI-H441_Bronchioloalveolar.Adenocarcinoma: METIS_p_NCLE_RNA1_Human_U133_Plus_2.0_E05_240954	14.87	16.62	49.04	34.08	87.71	212.35	48.29	18.77	24.56
H441 Lung_Cancer.Cell.Line_Large_NCI-H441_Bronchioloalveolar.Adenocarcinoma: GSM274741	16.59	14.5	38.25	45.12	72.27	119.51	47.77	26.89	22.77
H441 Lung_Cancer.Cell.Line_Large_NCI-H441_Bronchioloalveolar.Adenocarcinoma: GSM274742	14.95	15.78	44.38	37.62	71.5	116.88	44.24	25.52	21.04
H441 Lung_Cancer.Cell.Line_Large_NCI-H441_Bronchioloalveolar.Adenocarcinoma: NCI-H441_SS475525_HG-U133_Plus_2_HCHP-225837_	15.89	18.07	48.6	28.07	69.86	263.85	43.29	23.61	28.88
H441 Lung_Cancer.Cell.Line_Large_NCI-H441_Bronchioloalveolar.Adenocarcinoma: NCI-H441_SS475527_HG-U133_Plus_2_HCHP-225839_	19.1	16.67	50.57	27.93	68.59	226.22	44.21	26.03	27.01
H520 Lung_Cancer.Cell.Line_Large_NCI-H520_Squamous.Cell.Carcinoma: BRAKE_p_NCLE_RNA2_HG-U133_Plus_2_D02_241116	19.37	17.66	59.98	28.5	76.65	67.04	44.04	33.57	34.41
H520 Lung_Cancer.Cell.Line_Large_NCI-H520_Squamous.Cell.Carcinoma: GSM274798	16.5	15.8	48.05	30.93	78.98	87.21	46.82	36.39	21.66
H520 Lung_Cancer.Cell.Line_Large_NCI-H520_Squamous.Cell.Carcinoma: GSM274831	20.61	16.66	47.85	34.97	77.36	82.98	45.82	32.57	25.09
H522 Lung_Cancer.Cell.Line_Large_NCI-H522_Adenocarcinoma: NIECE_p_NCLE_RNA3_HG-U133_Plus_2_B08_296028	14.91	17.14	42.85	31.33	98.42	94.97	57.63	24.73	21.26
H522 Lung_Cancer.Cell.Line_Large_NCI-H522_Adenocarcinoma: GSM274753	17.07	17.13	48.65	38.8	86.16	65.48	48.6	28.98	23.56
H522 Lung_Cancer.Cell.Line_Large_NCI-H522_Adenocarcinoma: GSM274754	16.1	15.3	42.23	36.5	81.83	76.29	53.99	31.59	21.85
H522 Lung_Cancer.Cell.Line_Large_NCI-H522_Non-Small.Cell.Lung.Carcinoma: NCI-H522_SS181856_HG-U133_Plus_2_HCHP-167900_	14.4	16.48	43.98	22.48	68.53	77.74	70.22	20.51	22.26
H522 Lung_Cancer.Cell.Line_Large_NCI-H522_Non-Small.Cell.Lung.Carcinoma: NCI-H522_SS181857_HG-U133_Plus_2_HCHP-167901_	15.77	16.37	39.13	22.04	110.03	67.85	54.42	22.81	23.76

SUPPLEMENTARY FIGURE S1

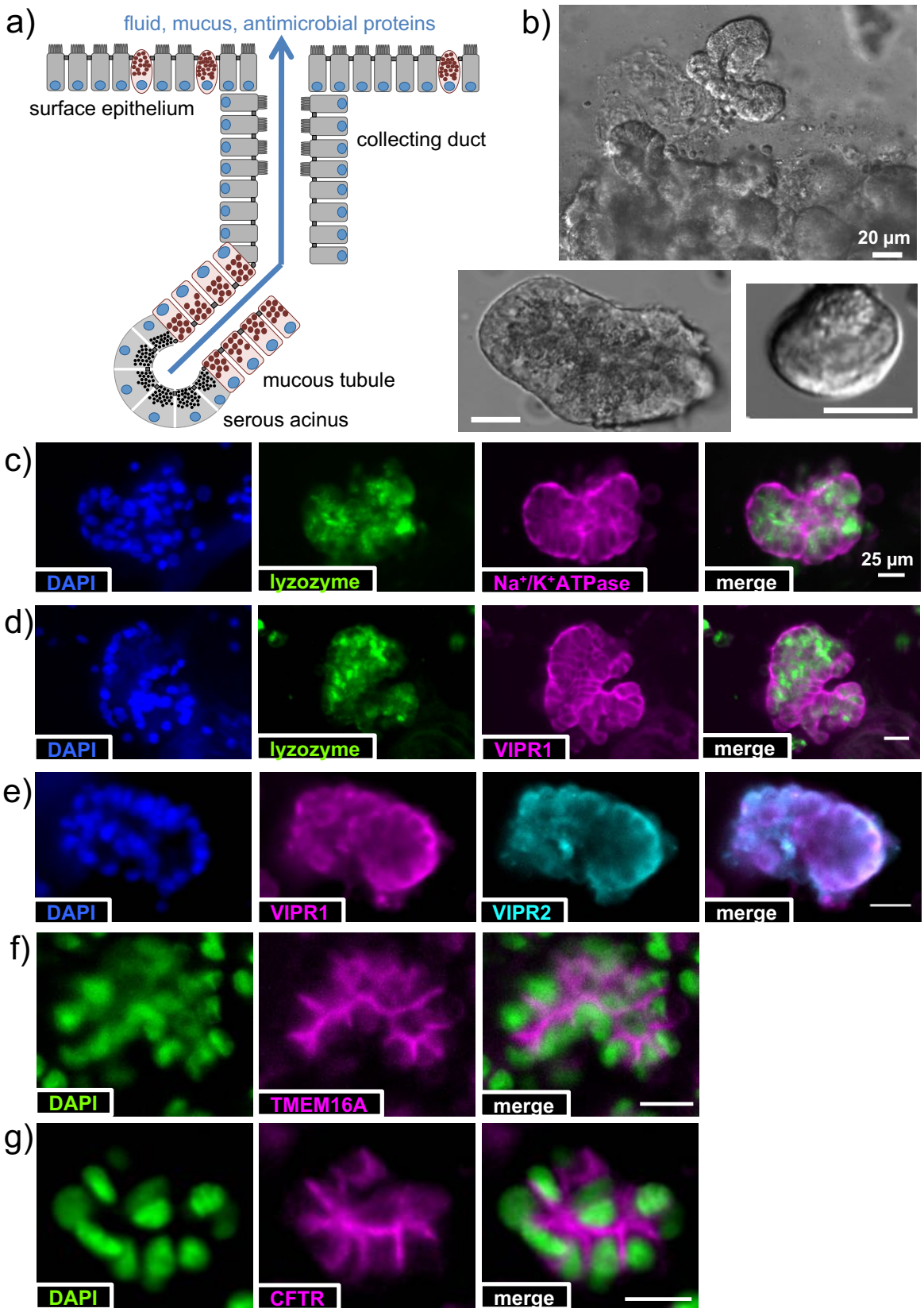

SUPPLEMENTARY FIGURE S1 Isolated airway serous acinar cells. **a)** Representative diagram showing serous acinar cells at the distal ends of submucosal glands, which secrete the bulk of fluid in response to agonists that utilize cAMP or Ca^{2+} as second messengers. **b)** Representative spinning disk confocal images of primary human serous acini and acinar cells isolated from human middle turbinate samples plated on CellTak coated coverslips. **c-e)** Isolated serous acini exhibited punctate granular immunofluorescence for lysozyme (*c*-*d*) as well as basolateral membrane staining for Na^+/K^+ ATPase (*c*), VIPR1 (*d*-*e*), and VIPR2 (*e*). **f-g)** Apical membrane staining was observed for secretory Cl^- channels TMEM16A (*f*) and CFTR (*g*), as previously described [3-6, 9]. Results are representative of immunofluorescence experiments using cells from ≥3 patients. Scale bars are 20 μm in *b* and 25 μm in *c*-*g*. CFTR, lysozyme, and TMEM16A immunofluorescence matched previous studies [3-6, 9] of airway submucosal gland serous cells.

SUPPLEMENTARY FIGURE S2

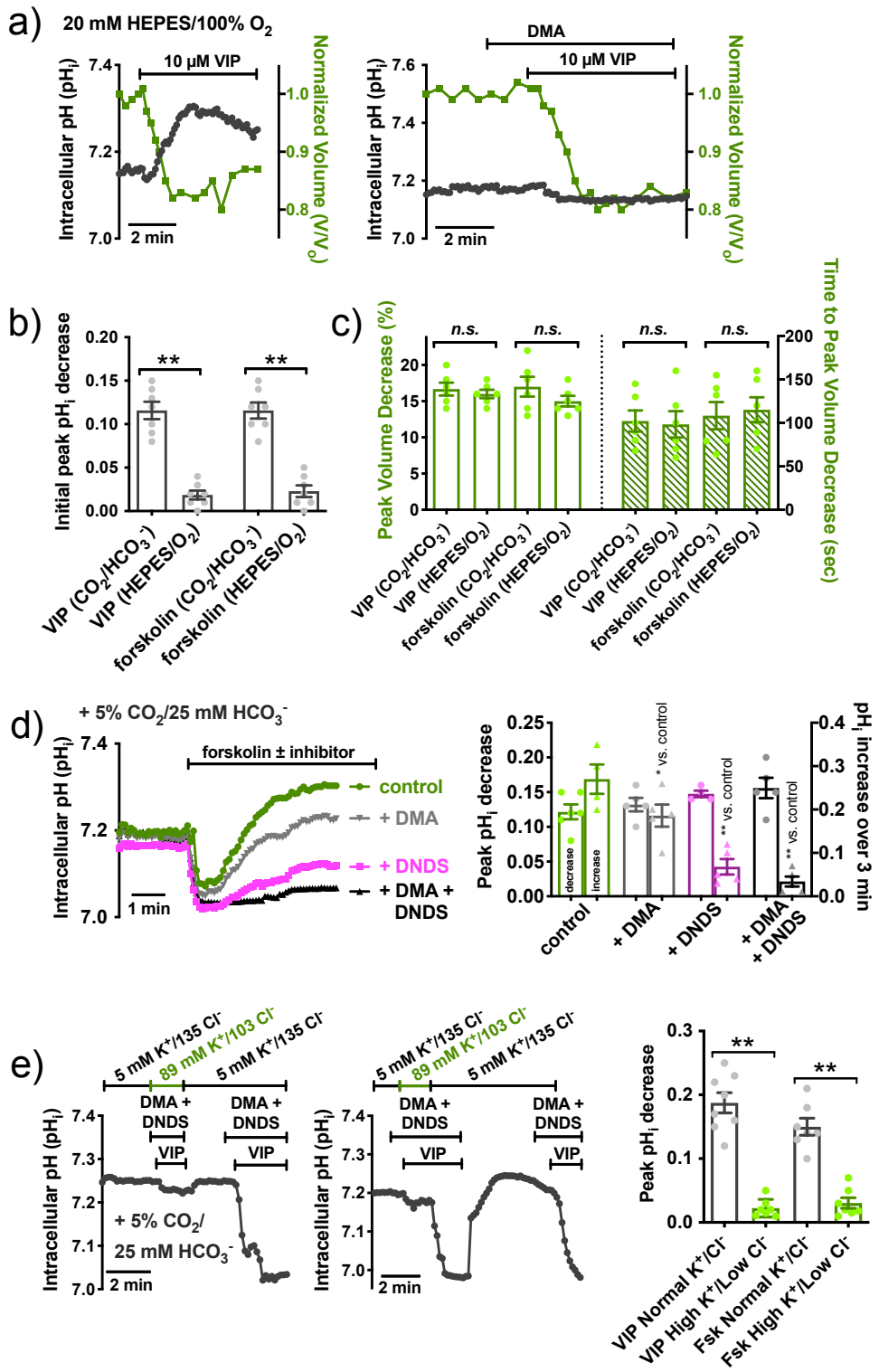

SUPPLEMENTARY FIGURE S2 VIP-induced acidification reflects conductive HCO_3^- efflux, while subsequent alkalinization reflects HCO_3^- uptake via $Na^+HCO_3^-$ cotransporter (NBC). **a)** In the absence of HCO_3^- (20 mM HEPES-buffered conditions gassed with 100% O_2), VIP-induced acidification is eliminated. However, cells still shrink at a normal magnitude and rate. Residual pH_i increase is blocked by DMA, suggesting it reflects NHE activity. **b-c)** Bar graphs (mean ± SEM) showing peak pH_i decrease (*b*) or volume decrease magnitude and kinetics (*c*) during VIP or forskolin stimulation in the presence or absence of CO_2/HCO_3^-. Significance determined by one-way ANOVA with Bonferroni posttest; $^{**}p < 0.01$ and *n.s.* = no statistical significance. These data demonstrate that VIP-induced pH_i decrease requires HCO_3^-, suggesting it reflects HCO_3^- efflux. However, the magnitude of initial cell shrinkage is not HCO_3^- -dependent; as previously shown, shrinkage primarily reflects Cl^- efflux [3-6, 8, 9]. This is likely due to the relative magnitude of Cl^- and HCO_3^- solute lost during secretion. A serous cell has resting $[Cl^-]_i$ = ~65 mM (supplementary figure S19 and [3]) and loses >50% of cellular Cl^- content (>40 meq•L^{-1}) during ~20% volume decrease [3, 33]. However, the actual HCO_3^- content lost from the cell during secretion is smaller; a 7.2 to 7.0 pH_i change would drop $[HCO_3^-]_i$ from ~16 mM to 12 mM (calculated via Henderson Hasselbach). Taking into account the cell volume loss (20%) but ignoring non-osmotically active volume for simplicity, this is a loss of cellular HCO_3^- content of (1 x 16 meq•L^{-1}) – (0.8 x 12 meq•L^{-1}) = ~6.4 meq•L^{-1} HCO_3^-. Thus, cell volume is primarily an indicator of Cl^- secretion while pH_i is primarily an indicator of HCO_3^-, as previously observed [4, 53]. **d)** In the presence of HCO_3^-, serous cell pH_i increases (after initial decrease) were substantially reduced by NBC inhibitor 4,4'-dinitrostilbene-2,2'-disulfonic acid (DNDS; 100 µM). Alkalinization was not significantly reduced by Na^+/H^+ exchanger (NHE) inhibitor dimethyl amiloride (DMA; 30 µM) alone. All experiments done at 37°C in the presence of 5% CO_2. Representative traces shown on left. Bar graph right shows mean ± SEM; ** = p <0.01 by one-way ANOVA with Bonferroni posttest. These data suggest NBC drives serous cell alkalinization during VIP stimulation, likely as a way to sustain HCO_3^- secretion due the basolateral localization of NBC in exocrine acinar cells [54-58], similar to what was previously observed with NHE sustaining HCO_3^- secretion during cholinergic-evoked secretion [4]. By keeping $[HCO_3^-]_i$ elevated during VIP stimulation, basolateral NBC will increase the driving force for HCO_3^- efflux across the apical membrane through CFTR. **e)** In the presence of high K^+/low Cl^- conditions designed to block conductive HCO_3^- efflux by clamping $E_{K+} = E_{Cl-} = E_{HCO3-} = V_m$ (described in the supplementary methods and [4]), VIP-induced acidification is blocked. Bar graph in *b* shows mean ± SEM with significance ($^{**}p<0.01$) determined via Student's *t* test. DMA (30 µM) + DNDS (100 µM) were used to prevent alkalinization so we could observe only the acidification (HCO_3^- efflux). Thus, the VIP-induced acidification likely reflects conductive HCO_3^- efflux, likely through an ion channel like CFTR and not a Cl^-/HCO_3^- exchanger.

SUPPLEMENTARY FIGURE S3

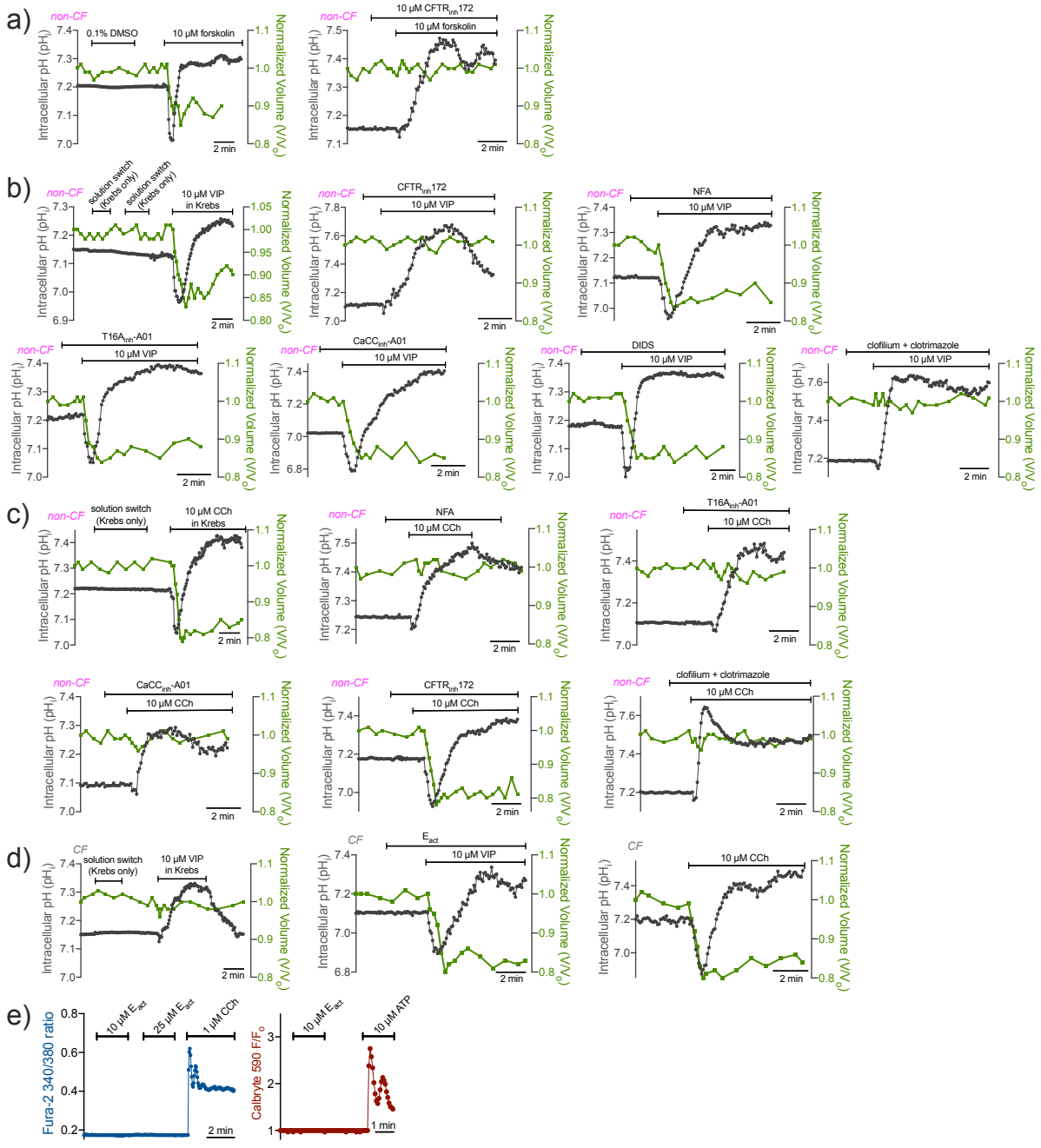

SUPPLEMENTARY FIGURE S3 Representative traces of responses summarized in main text figure 1. **a)** Representative traces of responses summarized in figure 1e. **b)** Representative traces of responses summarized in main text figure 1f. **c)** Representative traces of responses summarized in figure 1g. **d)** Representative traces of responses summarized in main text figure 1h. **e)** Eact was recently suggested to be an indirect activator of TMEM16A via TRPV4 activation and elevation of Ca^{2+} [59]. Serous cells were loaded with either fura-2 or Calbryte 590 by incubation in the AM ester form for 20 min as described [3, 5, 6] and imaged using fura-2 or TRITC filter sets, respectively. No evidence of changes in $[Ca^{2+}]_i$ were observed with concentrations of E_{act} used in this study, despite changes with sub-saturating cholinergic or purinergic stimulation. Traces are representative of experiments using 3-5 serous acini from 3 individual patients (9-15 experiments total with each dye). Two dyes were used to confirm no effects on $[Ca^{2+}]_i$.

SUPPLEMENTARY FIGURE S4

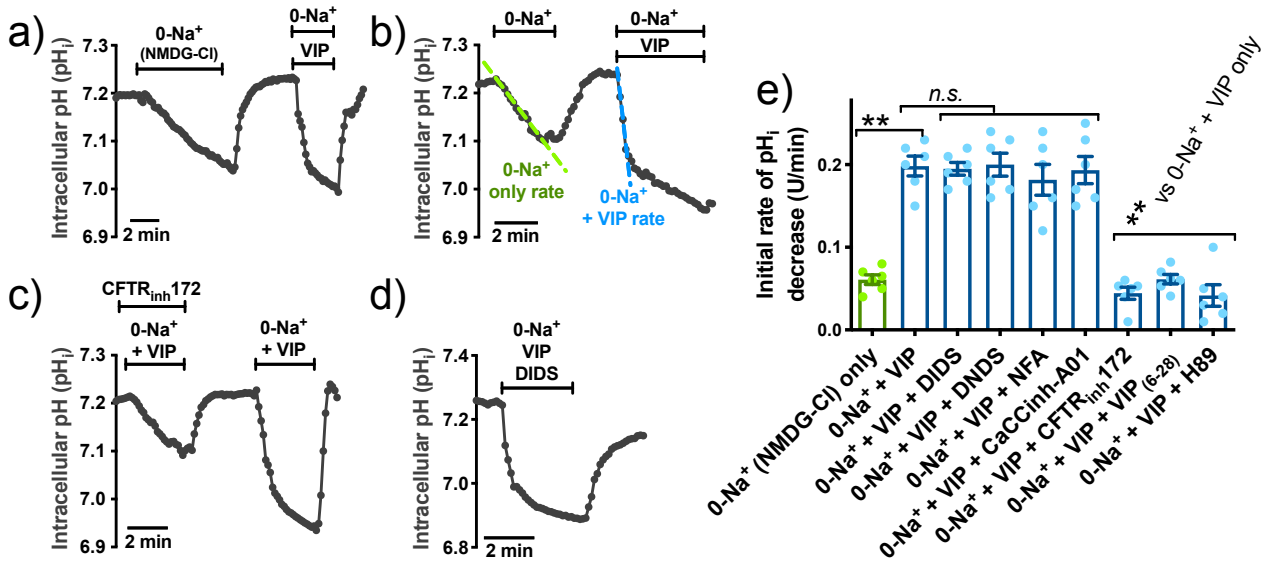

SUPPLEMENTARY FIGURE S4 Isolation of the VIP-induced HCO_3^- efflux pathway under 0-Na^+ conditions. **a-b)** To better isolate VIP-induced acidification, we performed experiments in 0-Na^+ to prevent alkalinization by Na^+ dependent mechanisms (NHE, NBC) in serous cells from non-CF patients. In the absence of Na^+ (isosmotic substitution with $NMDG^+$; solutions used described in the supplementary methods and [4]), cells exhibited a slow acidification. VIP (1 μM) nonetheless still increased the acidification rate under these conditions. Panel *B* shows comparisons of rates ± VIP (blue vs green). **c-d)** The VIP-induced increased in acidification was inhibited by $CFTR_{inh}172$ (20 μM; *c*), but not by Ca^{2+}-activated Cl^- channel (CaCC) and/or Cl^-/HCO_3^- exchanger (e.g., pendrin [60]) inhibitors like 4,4'-diisothiocyano-2,2'-stilbenedisulfonic acid (DIDS; *d;* 1 mM), DNDS (30 μM), NFA (100 μM), or $CaCC_{inh}$-A01. **e)** Bar graphs showing rates measured from experiments as in *A-D*. VIP-induced acidification was inhibited only by $CFTR_{inh}172$, VIP receptor antagonist $VIP_{(6-28)}$, or PKA inhibitor H89 (10 μM). Graph shows mean ± SEM with significance determined by one-way ANOVA with Bonferroni posttest; $^{**}p<0.01$ and *n.s.* = no statistical significance. All experiments done at 37°C in 5% CO_2/25 mM HCO_3^-. These data show that inhibitors of TMEM16A/CaCC [61-63] or pendrin [60] do not inhibit VIP-induced acidification. Along with ion substitution (**supplementary figure S1**) and data from CF patient cells (**figure 1**), these data support CFTR conduction as the primary HCO_3^- efflux pathway in serous cells during VIP stimulation.

SUPPLEMENTARY FIGURE S5

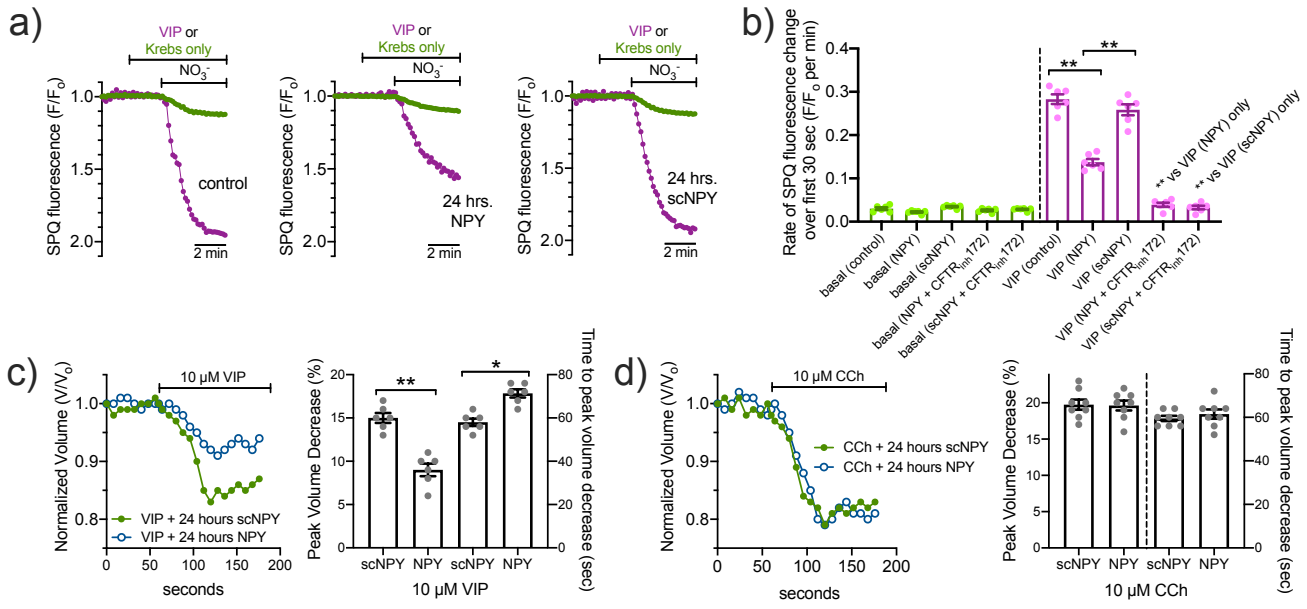

SUPPLEMENTARY FIGURE S5 Effects of 24 hours NPY stimulation on Cl- ion transport phenotypes. **a)** Representative traces of SPQ fluorescence from isolated serous cells in the presence of 5 μM VIP after 24 hrs prior stimulation with media only (control), 1 μM NPY, or scrambled NPY (scNPY). Cells were isolated and plated on Matrigel-coated coverslips (1:30 dillution of growth factor reduced Matrigel) and stimulated in serum-free MEME for 24 hours. Cells were loaded with SPQ 2 hours prior to the experiments, done in the continued presence of NPY or scNPY as applicable. Unstimulated SPQ fluorescence (no VIP) changes are shown in green and VIP-stimulated fluorescence changes shown in magenta (separate experiments). As described in the text, supplementary methods, and previous studies [3-6, 9, 11, 14], SPQ is quenched by Cl^- but no NO_3^-. Upon substitution of extracellular Cl^- for NO_3^-, intracellular [Cl^-] decreases via electroneutral exchange of Cl^- for NO_3^- via diffusion and SPQ fluorescence increases. As most Cl^- channels have roughly equal permeability to Cl^- and NO_3^-, the relative rate of SPQ fluorescence change is roughly equal to relative anion permeability. **b)** Bar graph showing initial rate of SPQ fluorescence change over first 30 sec of NO_3^- substitution. NPY, but not scNY, significantly reduced SPQ fluorescence changes under VIP-stimulated conditions but not unstimulated conditions. Data points for each bar are 6 independent experiments using cells from 3 patients (2 experiments per patient); $^{**}p$ <0.01 by 1-way ANOVA with Bonferroni posttest. **c)** Cells were stimulated with NPY or scNPY as above and then VIP cell volume responses were immediately imaged in the continued presence of NPY or scNPY (representative traces from independent experiments shown on left). The peak cell shrinkage and time to peak shrinkage in response to 10 μM VIP was reduced in the presence of NPY (bar graph on right). d) Similar experiments were carried out as c but with stimulation with 10 μM CCh. No inhibition of secretion was observed with CCh. Significance in *c* and *d* by 1-way ANOVA with Bonferroni posttest with paired comparisons as indicated; $^{*}p$<0.05 and $^{**}p$<0.01. Data points for each bar are 6 independent experiments using cells from 3 patients (2 experiments per patient); $^{**}p$ <0.01 by 1-way ANOVA with Bonferroni posttest. Together with experiments in the main text, these data suggest NPY reduces anion secretion in response to cAMP-elevating VIP but does not affect anion secretion in response to CCh.

SUPPLEMENTARY FIGURE S6

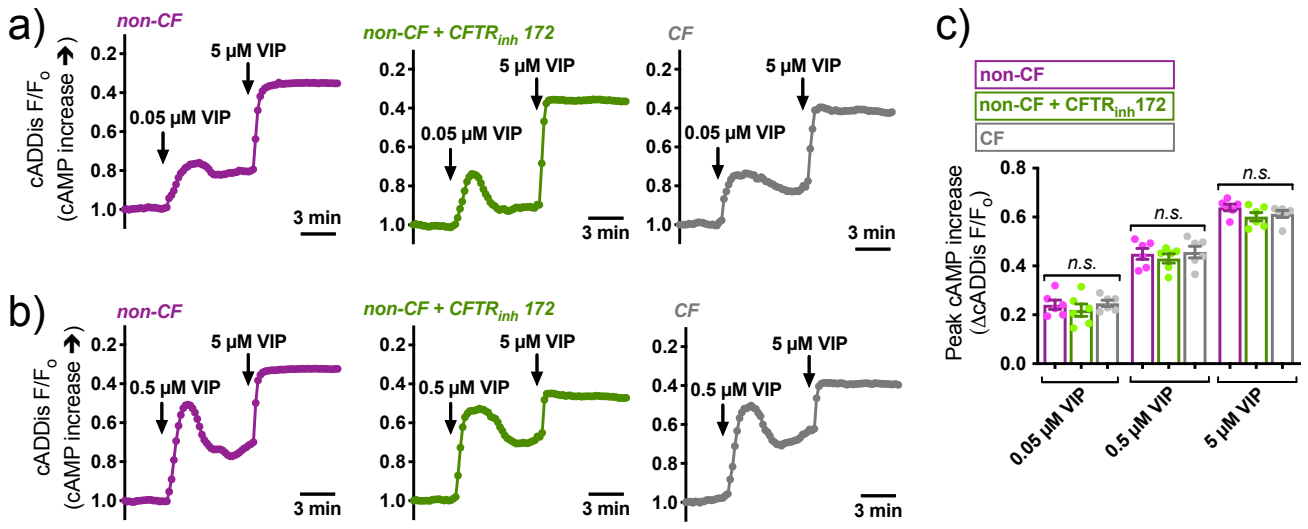

SUPPLEMENTARY FIGURE S6 Comparison of VIP-induced cAMP signaling in CF vs non-CF cells. CFTR has been proposed to act as a hub for kinases and other signaling proteins. We used a fluorescent cAMP biosensor to visualize VIP-activated cAMP increases in CF and non-CF serous cells. We utilized a baculovirus pseudotyped for mammalian cells (BacMam) vector [2], as BacMam was previously used to express proteins in primary lacrimal gland acinar cells [64-66]. Serous acinar cells were isolated, seeded onto CellTak-coated coverslips, and transduced for 6 hrs with a BacMam expressing an mNeonGreen-based fluorescent cAMP biosensor (downward cADDis; Montana Molecular, Bozeman MT; [1]) under a CMV promotor followed by 18-24 hrs incubation. Single transduced cells and acini were imaged using GFP filters. A decrease in F/F_o (plotted inversely, thus shown as an upward deflection of trace) equals an increase in cAMP (as indicated by the arrow on the axis). **a-b)** We examined if CF serous cells exhibited alterations in cAMP signaling in response to 0.05, 0.5, and 5 µM VIP. No differences were observed between CF and non-CF patients. This suggests that VIP-evoked cAMP signaling, at least at a global cytoplasmic level, is intact in CF serous cells. We also treated non-CF cells with $CFTR_{inh}172$, and found no alterations of cAMP signals. **c)** Bar graph of peak responses (absolute values are plotted) from representative experiments as shown in *a-b* (3-5 patients samples used for each group, ≥2 experiments per patient per group). 1-way ANOVA with Bonferroni posttest suggested no statistically significant differences. Bar graph shows mean ± SEM; *n.s.* = no statistical significance.

SUPPLEMENTARY FIGURE S7

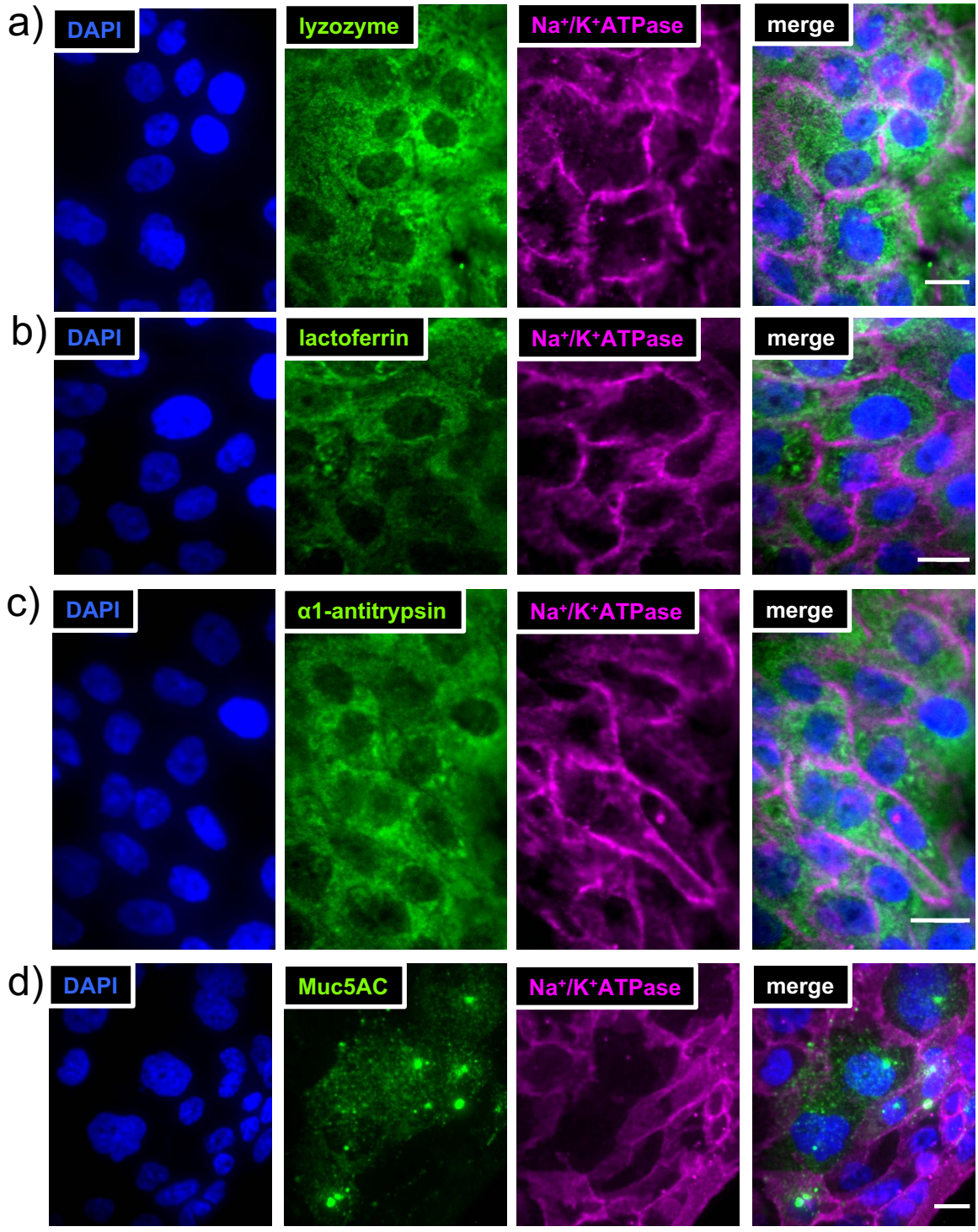

SUPPLEMENTARY FIGURE S7 Expression of serous cell markers lysozyme (*a*), lactoferrin (*b*), and alpha-1-antitrypsin (*c*) in Calu-3 cells as well as goblet cell marker Muc5AC (*d*). Cells were seeded and grown as a monolayer on collagen coated glass bottom dishes (MatTek), and confluent monolayers were fixed in ice cold MeOH for 3 min before immunostaining as described in the supplementary methods. Antibody against Na^+/K^+ ATPase was used as a positive plasma membrane control.

SUPPLEMENTARY FIGURE S8

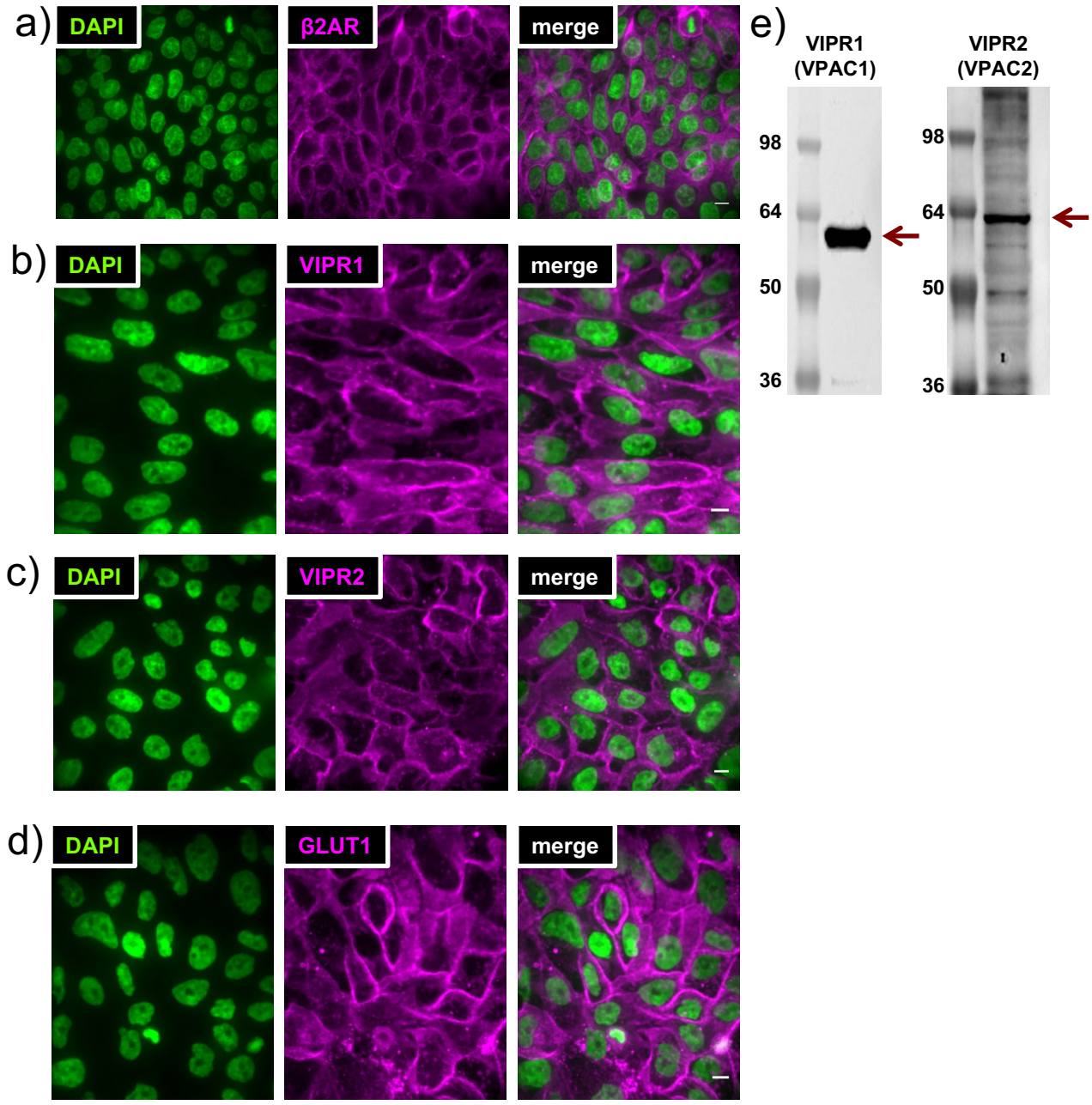

SUPPLEMENTARY FIGURE S8 Expression of both VIPR1 (VPAC1) and VIPR2 (VPAC2) in Calu-3 cells. **a-d)** Cells were seeded and grown as a monolaryer on collagen coated glass bottom dishes (MatTek), and confluent monolayers were fixed in ice cold MeOH for 3 min before immunostaining as described in the supplementary methods. GLUT1 and β2AR1 were used as plasma membrane controls. **e)** Western blot showing bands corresponding to VIPR1 and VIPR2 using antibodies from *b* and *c* and as used in the main text.

SUPPLEMENTARY FIGURE S9

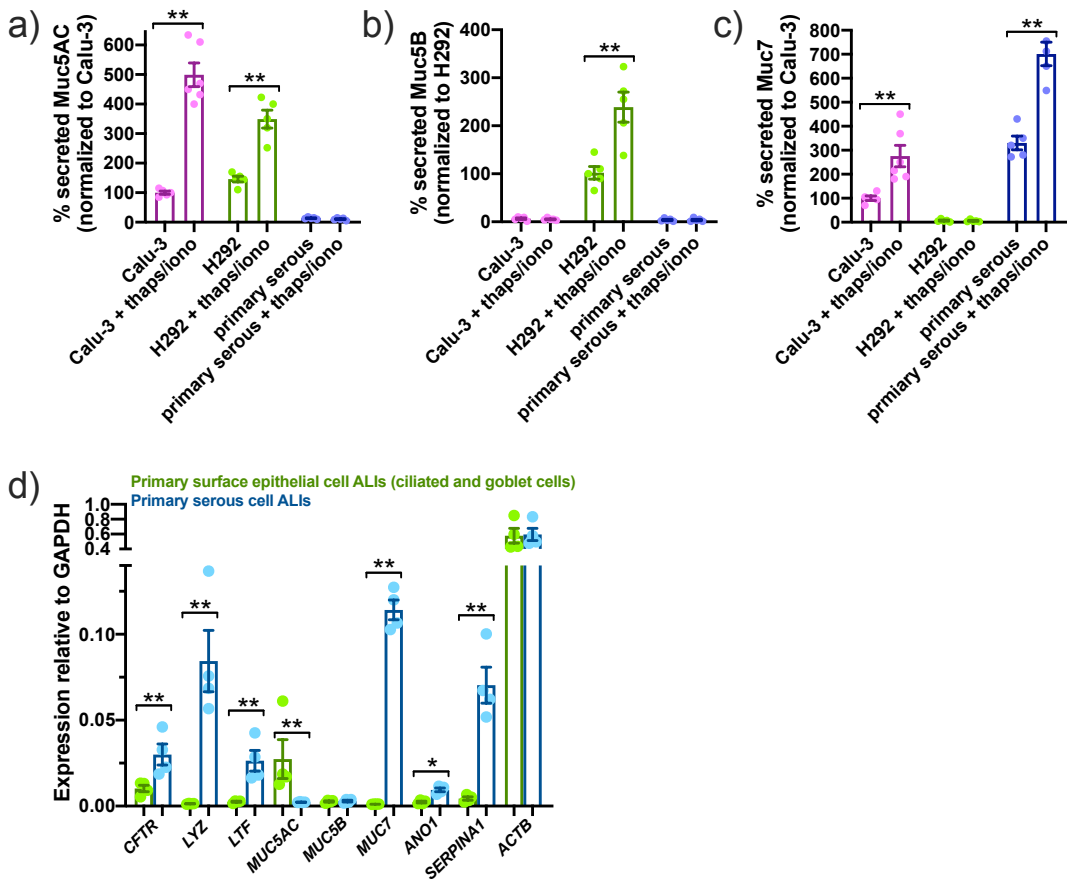

SUPPLEMENTARY FIGURE S9 Verification of Muc7, but not Muc5AC or Muc5B, production from primary human nasal serous cell cultures, suggesting maintenance of serous phenotype. ASL was collected ± stimulation with thapsigarin and ionomycin (10 µg/ml each; 30 min, basolaterally) to maximally elevate Ca^{2+} and activate acute secretion. **a)** Calu-3 cells produced goblet cell Muc5AC [67] as previously reported [68-70], as did H292 cells, as previously reported [71-74]. **b)** H292 cells produced mucous cell-marker Muc5B [75, 76], as previously reported [77-80]. Calu-3 and serous cells did not make detectible Muc5B. **c)** Both Calu-3 and primary serous cells produced serous cell marker Muc7 [75, 76]. H292 cells did not. Secretion of all mucins was increased acutely after basolateral stimulation with thapsigargin and ionomycin. **d)** Primary surface epithelial cells (cultured as described [13, 14, 19, 20] to generate primarily ciliated and goblet cells) and serous cells were cultured from the same patients for three weeks after air exposure. Expression of CFTR, lysozyme (LYZ), lactoferrin (LTF), Muc5AC, Muc5B, Muc7, Ano1 (TMEM16A), alpha-1-antrypsin (SERPINA1), and actin were compared with GAPDH. Serous cell cultures expressed higher levels of CFTR and serous cell markers lysozyme, lactoferrin, alpha-1-antitrypsin, and Muc7 than surface epithelial cells. Surface epithelial cells expressed higher levels of goblet cell Muc5AC. Mucous cell Muc5B was not expressed at high levels in either type of culture. All data are mean ± SEM of 3-5 independent experiments using primary serious cells from 3-5 separate non-CF patients.

SUPPLEMENTARY FIGURE S10

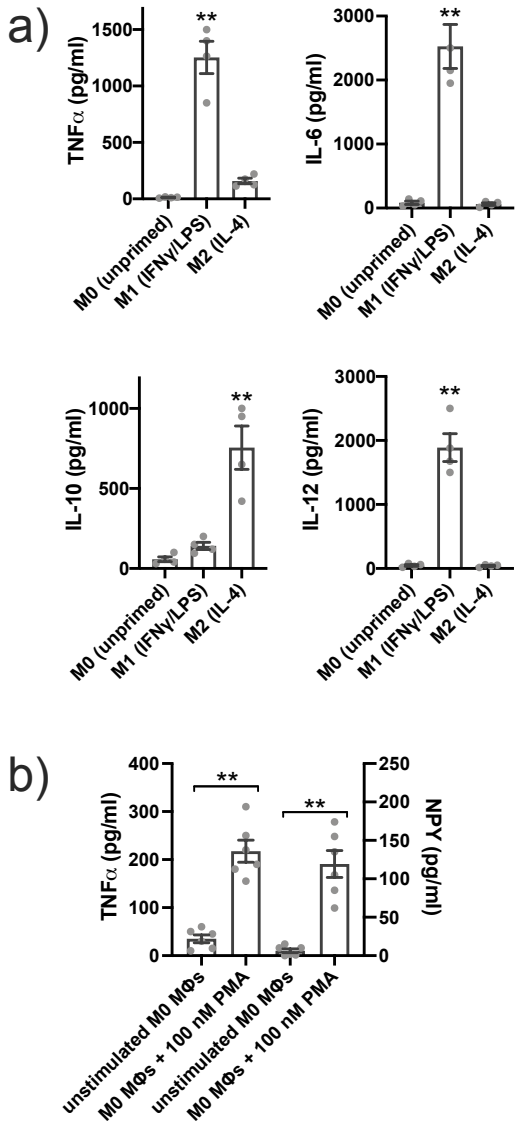

SUPPLEMENTARY FIGURE S10 Confirmation of macrophage (Mϕ) differentiation by production of appropriate cytokines in response to M1 vs M2 polarization. **a)** Human monocyte-derived Mϕ were cultured as described in the text, and stimulated as indicated in the graphs for the final 3 days of the 10 day differentiation. M1 polarization (IFN γ + LPS [81, 82]) resulted in robust secretion of TNFα, IL-6, and IL-12, while M2 polarization (IL-4 [81, 82]) resulted in robust secretion of IL-10, as determined by ELISA. **b)** Stimulation of M0 (unpolarized) Mϕs by PMA for 48 hrs. resulted in secretion of TNFα (left two bars) as well as NPY (right two bars), as previously reported [26, 83-86], as determined by ELISA. Add data are from 6 independent experiments from Mϕs isolated from 3 separate individuals (2 experiments per individual). Significance determined by 1-way ANOVA with Bonferroni posttest; ** $p<0.01$.

SUPPLEMENTARY FIGURE S11

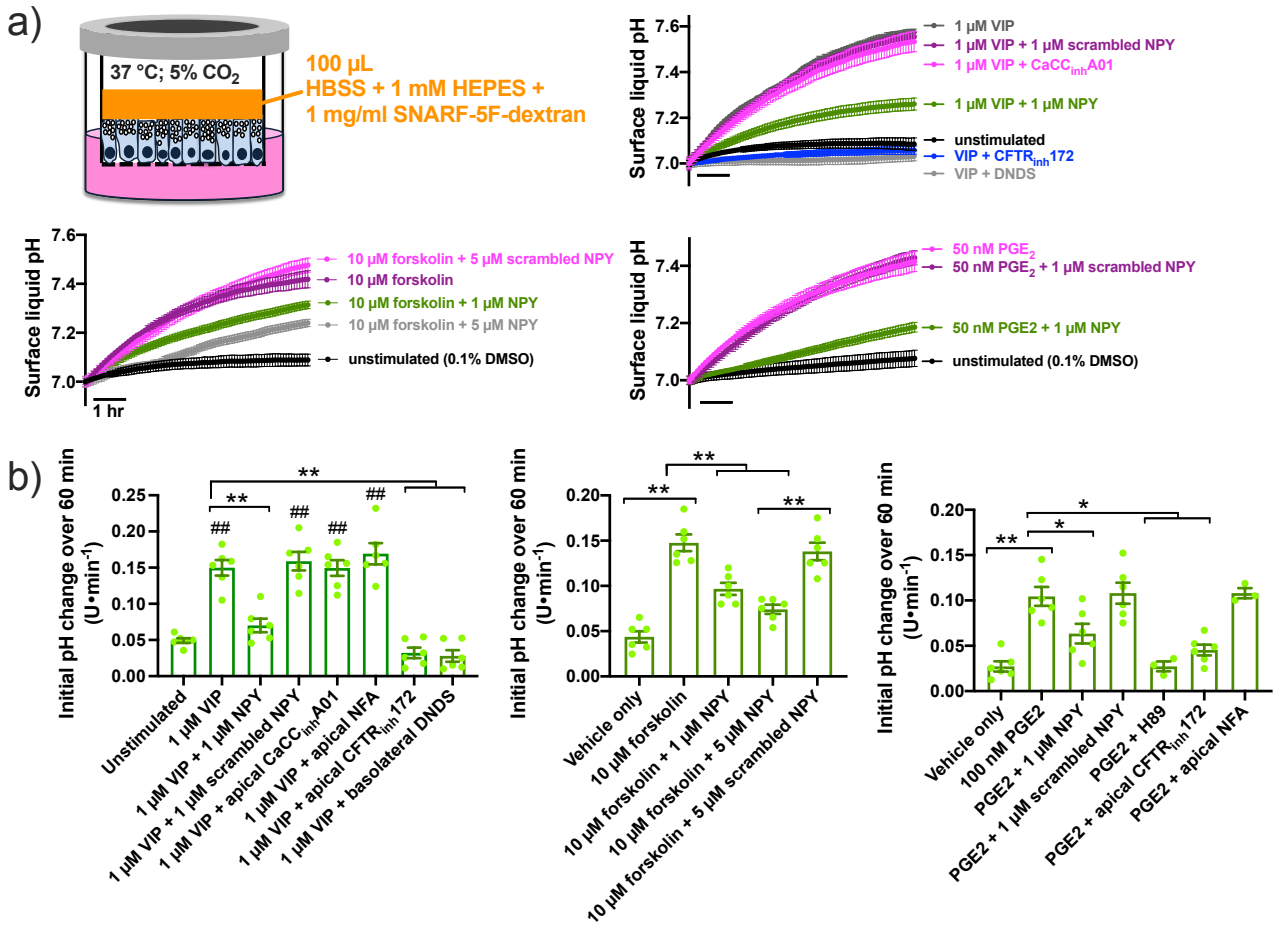

SUPPLEMENTARY FIGURE S11 VIP, forskolin, or prostaglandin E_2 (PGE_2) increased apical secretion of HCO_3^- over >8 hours, while NPY reduced secretion in response to all three agonists. **a)** Non-CF serous cell ALIs were imaged in a stage top incubator (Tokai Hit, Tokyo, Japan) at 37 °C with 5% CO_2. 100 uL of 1 mg/ml SNARF dextran in low buffering capacity solution was added (HBSS with 1 mM HEPES, as described [38]), and pH was measured every 10 min. These experiments facilitated addition of inhibitors to the apical side. Shown are representative traces (average of 3 ALIs, 3 fields per ALI) from single experiments. **b)** Bar graphs (mean ± SEM) of 6 individual experiments from ≥3 patients. Left bar graph shows inhibition of VIP-induced pH_i increase by NPY but not scrambled NPY as well as by $CFTR_{inh}172$ (15 µM) but not by apical TMEM16A inhibitors $CaCC_{inh}$-A01 (15 µm) or niflumic acid (NFA; 100 µM). Block by basolateral DNDS (25 µM) suggests surface liquid pH_i increases are due to HCO_3^- secretion sustained by $Na^+HCO_3^-$ co-transporter (NBC) activity. Middle bar graph shows reduction of forskolin-induced ASL pH_i increase by NPY but not scrambed NPY. Right bar graph shows inhibition of PGE_2-inducd HCO_3^- secretion by NPY, protein kinase A inhibitor H89 (10 µM), or $CFTR_{inh}172$. Significance determined by 1-way ANOVA with Bonferroni posttest; $^{**}p<0.01$ vs bracketed bars and $^{\#\#}p<0.01$ vs unstimulated control. These data support the hypothesis that cAMP-elevating agonists like VIP, forskolin, and PGE_2 activates HCO_3^- secretion through apical CFTR sustained by basolateral NBC and support results from the main text that NPY has an inhibitory effect on this process.

SUPPLEMENTARY FIGURE S12

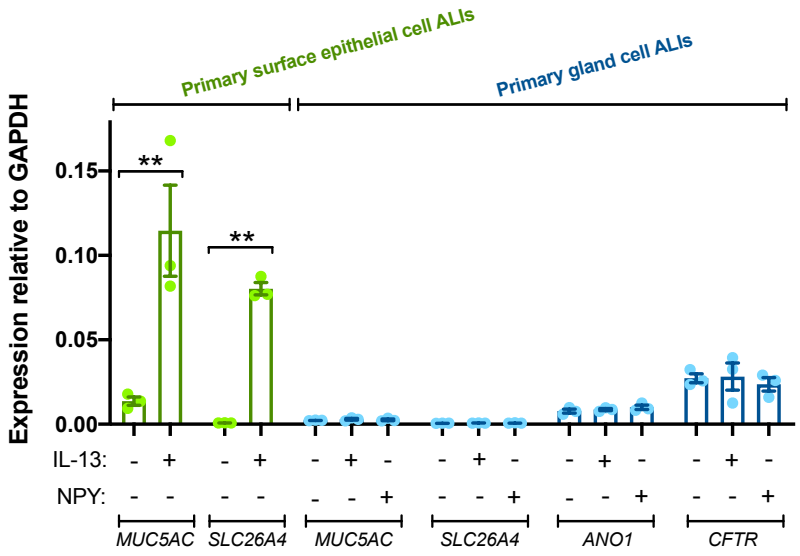

SUPPLEMENTARY FIGURE S12 Primary serous cell air-liquid interface (ALI) cultures or surface epithelial cell ALIs (primarily ciliated and goblet cells) were grown and stimulated with IL-13 or NPY as indicated in the figure and main text. Quantitative PCR was carried out for the indicated genes as described in the supplementary methods. Three ALIs from three individual patients were used for each condition as independent experiments. The same patients were used for surface epithelial and gland cultures. Significance determined by Bonferroni posttest with paired comparisons; $^{**}p<0.01$.

SUPPLEMENTARY FIGURE S13

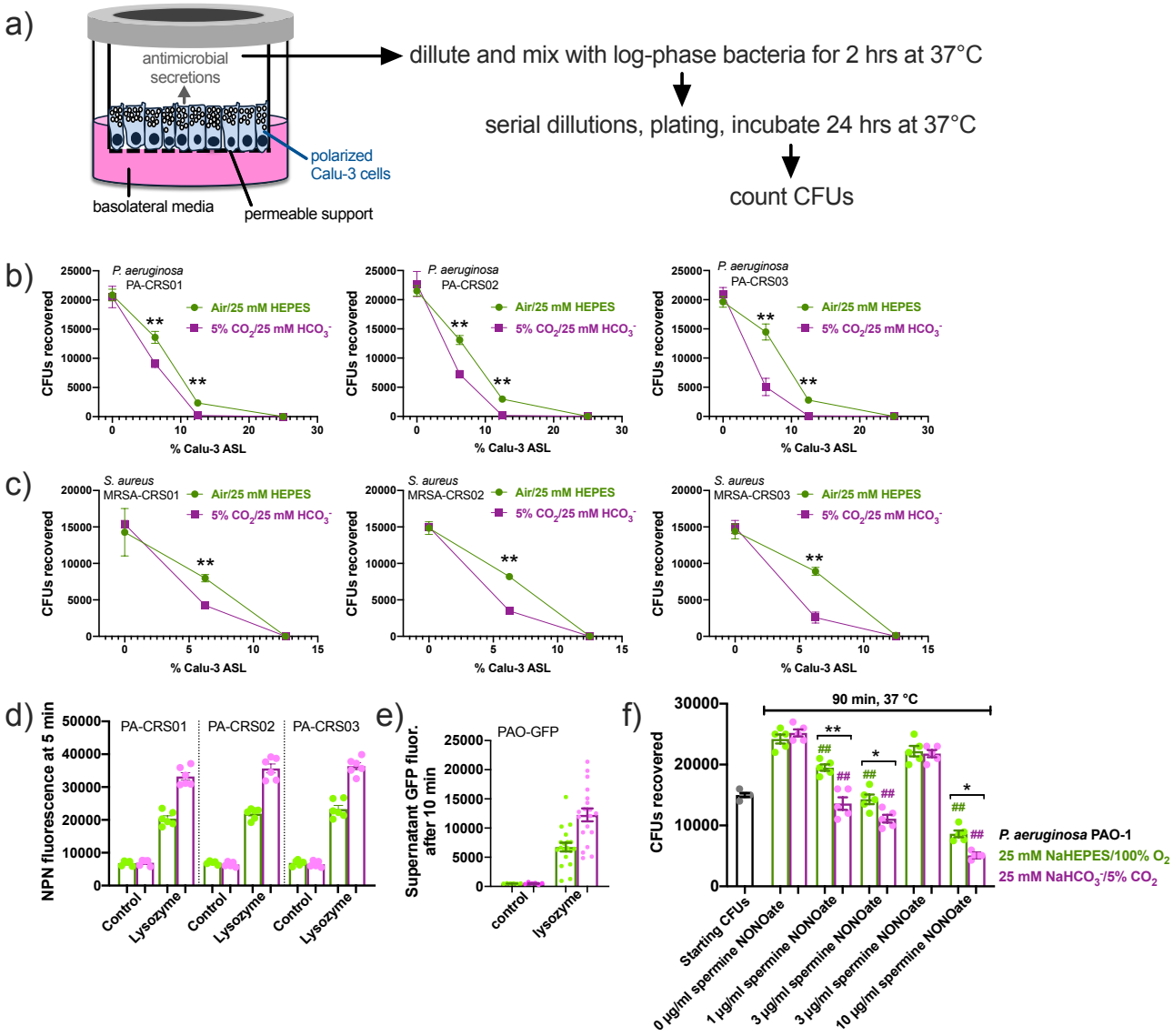

SUPPLEMENTARY FIGURE S13 HCO_3^- increases antimicrobial efficacy of Calu-3 secretions against clinical *Pseudomonas aeruginosa* strains isolated from chronic rhinosinusitis (CRS) patients. HCO_3^- has been suggested to be critical to efficacy of antimicrobial peptides secreted by serous cells [8, 87-91]. Antimicrobial assays were carried out as described ([40] modified from [45]) using ASL from Calu-3 bronchial cell cultures. **a-c)** Apical washings (collected with either 25% PBS + 20 mM HEPES or 25% PBS + 25 mM HCO_3^-) were mixed with clinical CRS isolates of *P. aeruginosa* (*b*) or methicillin-resistant *S. aureus* (*c*) and incubated at 37°C in room air (HEPES-buffered washings) or 5% CO_2 (HCO_3^--buffered washings) followed by serial dilutions and spotting on plates for CFU counting. At low dilutions (6.25-12.5%), antimicrobial activity was greater in the presence of 5% CO_2. **d)** NPN fluorescence (reflecting uptake due to cell wall damage) of clinical *P. aeruginosa* strains was measured after 5 min of lysozyme treatment (as described [40]) in the presence (pink) or absence of HCO_3^- (green). **e)** GFP-release of GFP-expressing *P. aeruginosa* (PAO-GFP) was measured during lysozyme treatment in the presence (pink) or absence (green) of HCO_3^-. **f)** *P. aeruginosa* lab type strain PAO-1 was mixed in the presence (pink) or absence (green) of HCO_3^- with various concentrations of NO donors, which have anti-bacterial effects (as described [92]). Overall, the presence of HCO_3^- had small but significant pro-bactericidal effect in all assays tested.

SUPPLEMENTARY FIGURE S14

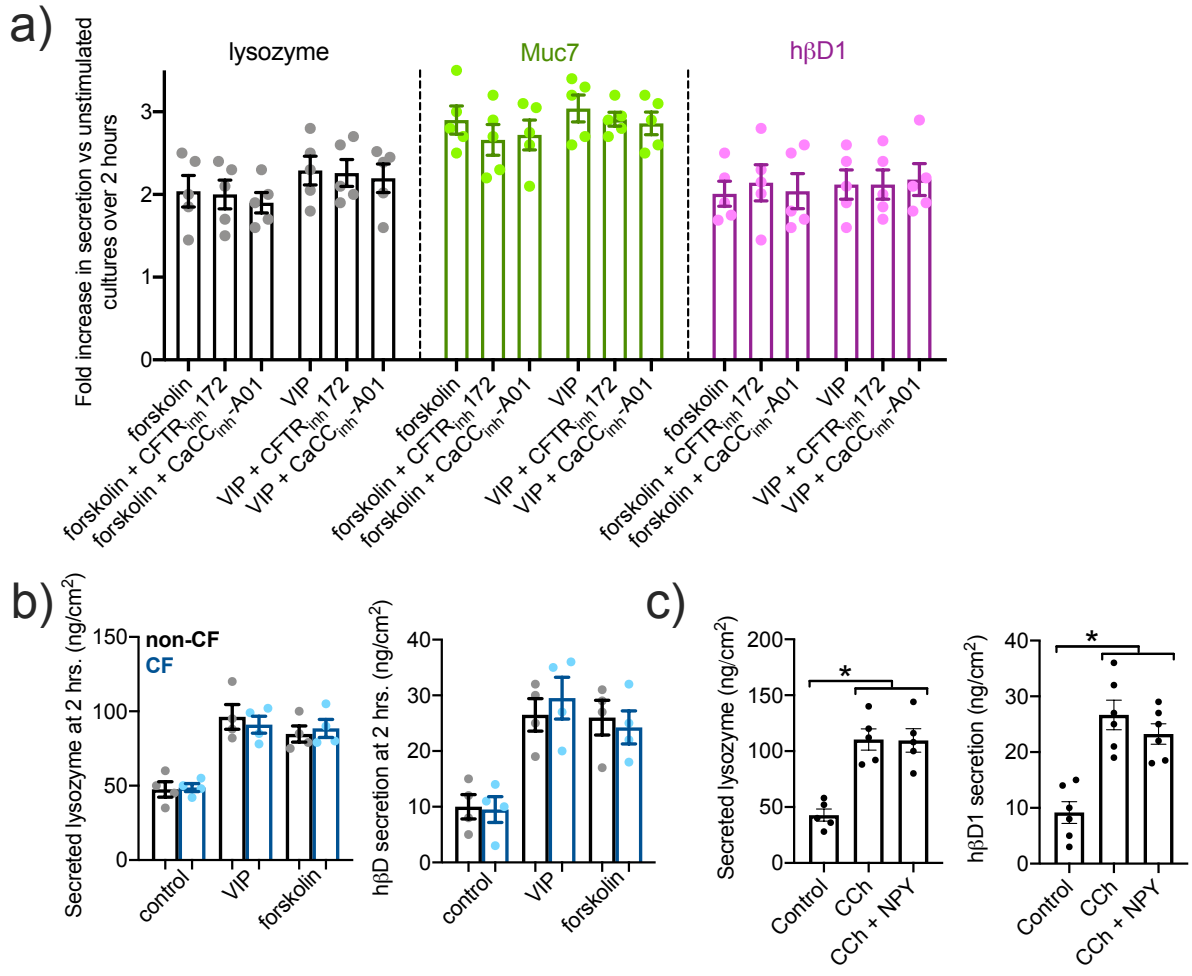

SUPPLEMENTARY FIGURE S14 **a)** Lysozyme, Muc7, and β-defensin 1 (hβD1) secretion was quantified by ELISA as in the main text. Fold increase in secretion from 5 individual experiments (using ALIs from 5 individual patients) was plotted. No significant reduction of secretion was observed to forskolin (10 μM) or VIP (5 μM) stimulation in the presence of apical $CFTR_{inh}172$ (10 μM) or $CaCC_{inh}$-A01 (10 μM), determined by one-way ANOVA with Bonferroni posttest. **b)** ALIs grown from non-CF (gray) or CF (blue) tissue were stimulated with VIP (5 μM) or forskolin (10 μM) and assayed for lysozyme or hβD1 as above. No difference was observed in baseline or stimulated secretion between CF and non-CF patients by 1-way ANOVA with Bonferroni posttest with paired comparisons. Data shown are from 4 independent experiments using ALIs from 2 CF and 2 non-CF patients (2 ALIs per patient per condition). **c)** Lysozyme and hβD1 were assayed after 2 hours stimulation with 10 μM carbachol (CCh), a cholinergic agonist that activates Ca^{2+}-dependent, TMEM16A-dependent, CFTR-independent secretion from serous cells (this study and [3-6, 8, 9]). No significant inhibition of secretion was observed with NPY (1 μM), determined by one-way ANOVA with Bonferroni posttest. Each condition shows data points from independent experiments using ALIs from separate individual patients (5 experiments per condition); *p<0.05.

SUPPLEMENTARY FIGURE S15

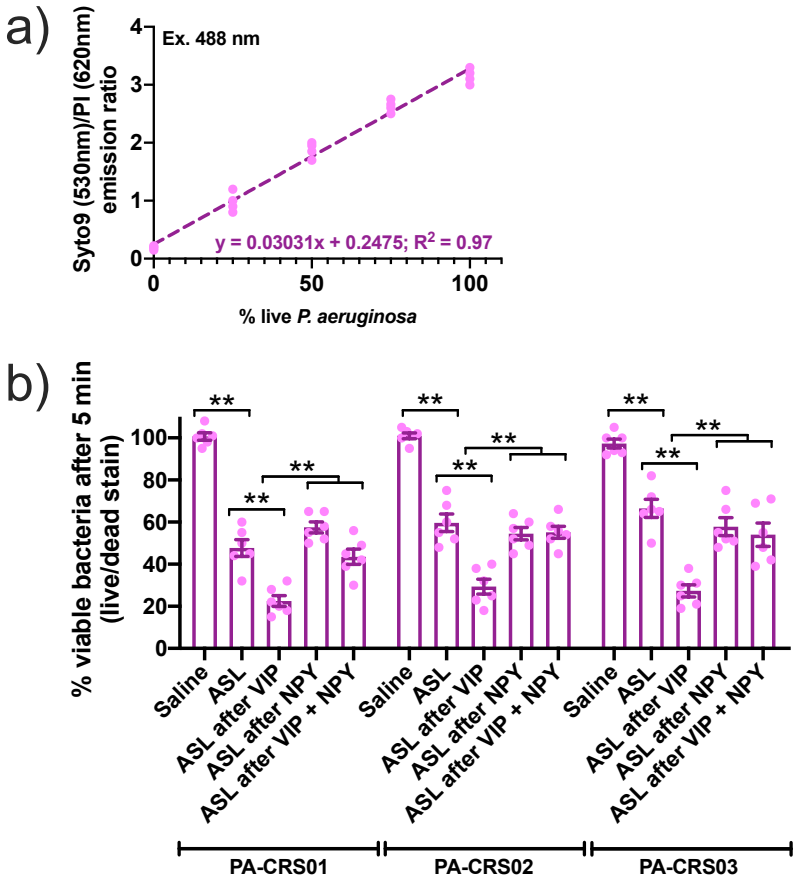

SUPPLEMENTARY FIGURE S15 Confirmation of neuropeptide-induced changes in ASL antimicrobial efficacy by live-dead staining. **a)** Incubation of dilutions of live and heat-killed P. aeruginosa (PAO-1) showed a linear relationship of Syto9 (live cell stain) and propidium iodide (PI; dead cell stain). Strain PA-CRS01 was used for calibration. **b)** Live bacteria were mixed with ASL washings from primary serious ALI cultures stimulated as indicated, stained with Syto9 and PI, and read on a plate reader using 488 nm excitation and ratiometric emission (530 and 620 nm). Calibration from *a* was used to convert fluorescence ratio into viability. Bar graph shows mean ± SEM from 5-6 independent experiments using ALI washings from ≥3 separate patients. Three clinical isolates of *P. aeruginosa* isolated from CRS patients were used. Significance determined by 1-way ANOVA with Bonferroni posttest; ***p*<0.01.

SUPPLEMENTARY FIGURE S16

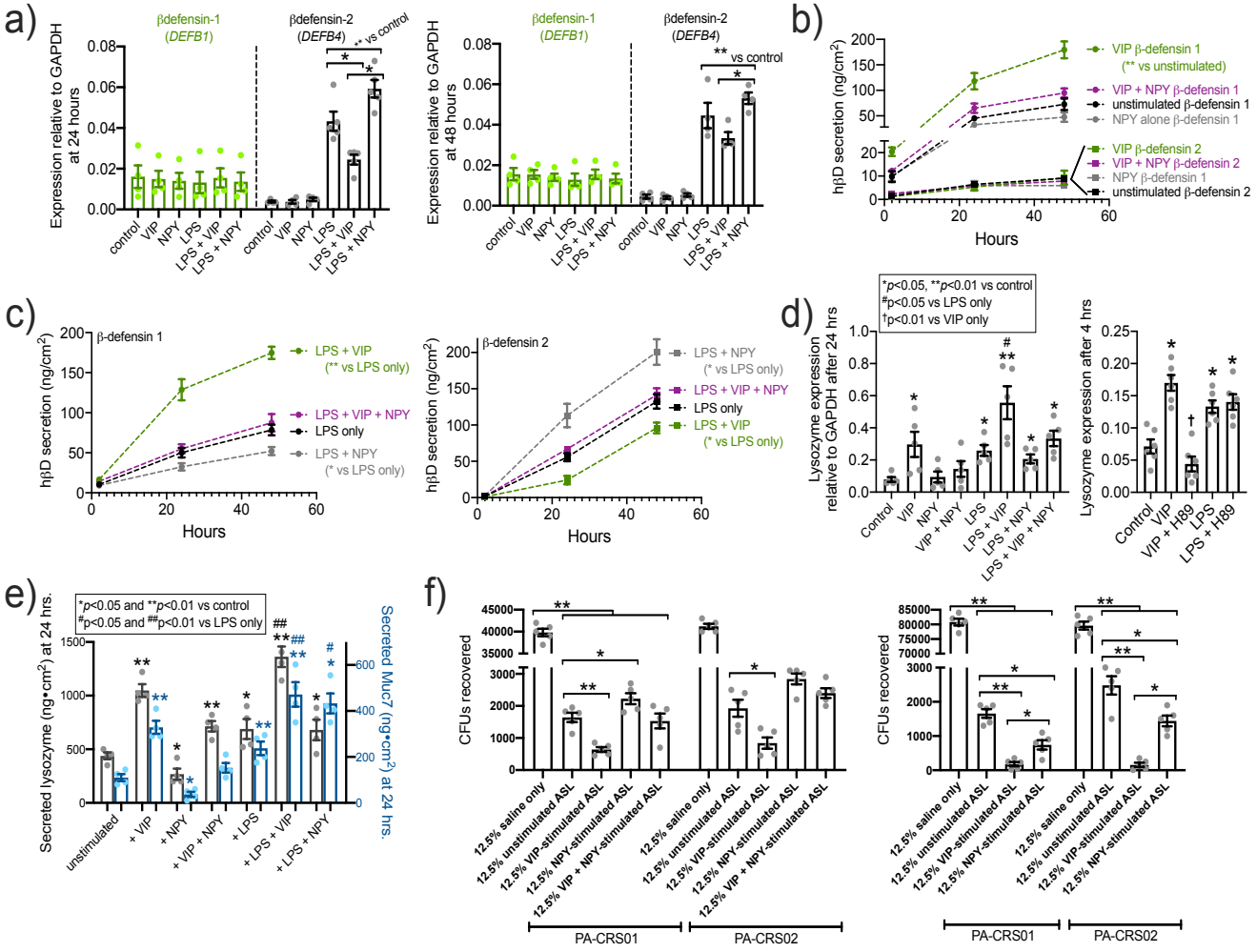

SUPPLEMENTARY FIGURE S16 Longer-term alterations of antimicrobial peptide production, secretion, and efficacy in serous ALI cultures. **a)** Expression of β-defensin 1 (*DEFB1* gene) and β-defensin 2 (*DEFB4* gene) was measured by qPCR TaqMan assay at 24 hours ± VIP, ± NPY, ± LPS (100 ng/ml). As expected, LPS increased NFκB-regulated β-defensin 2 but not constitutive β-defensin 1 [93, 94]. NPY (100 nM) and VIP (1 μM) had no effects on expression alone. VIP reduced β-defensin 2 expression at 48 hours. While LPS + NPY was significantly different from LPS + VIP conditions, LPS + NPY was not significantly different from LPS alone. Significance by 1-way ANOVA with Bonferroni posttest. Each bar graph shows mean ± SEM of 4 independent experiments using cultures from 4 different patients. **b)** Measurement of β-defensins 1 and 2 secretion into the ASL by ELISA as described in the methods and text. VIP increased secretion of β-defensin 1 over 48 hours (VIP $p<0.01$ vs unstimulated) while NPY eliminated the effect of VIP (VIP + NPY $p<0.01$ vs VIP alone). β-defensin 2 was not significantly increased by any stimulation. Significance determined by 1-way ANOVA with Bonferroni posttest comparing all points at 48 hours. Data are mean ± SEM of 4 independent experiments per condition per timepoint using cultures from 4 different patients. **c)** Measurement of β-defensins 1 and 2 secretion into the ASL by ELISA in the presence of LPS. LPS had minimal effect on β-defensins 1, but NPY reduced β-defensin 1 secretion ($p<0.05$ vs LPS only) while VIP enhanced it ($p<0.01$ vs LPS only). In contrast, LPS enhanced secretion of β-defensin 2, and this was further enhanced ($p<0.05$) with NPY + LPS. VIP reduced the effect of LPS on β-defensin 2 ($p<0.05$ vs LPS only). Significance determined by 1-way ANOVA with Bonferroni posttest comparing all points at 48 hours. Data are mean ± SEM of 4 independent experiments per timepoint per condition using cultures from 4 different patients. **d)** Left bar graph: lysozyme expression was measured ±VIP ±NPY ±LPS. VIP increased expression of lysozyme while VIP + NPY together did not increase lysozyme expression over control (unstimulated). LPS also increased lysozyme expression, and this was potentiated by VIP but not NPY. Right bar graph: Increase of lysozyme expression by VIP was inhibited by H89 (1 μM) while increase in response to LPS was not. This suggest that effects of VIP may be mediated by cAMP-activated transcription factor CREB, which can increase lysozyme transcription [95, 96]. Significance determined by 1-way ANOVA with Bonferronni posttest comparing all points at 48 hours. Data are mean ± SEM of 5 independent experiments using cultures from 5 different patients for each time point. **e)** Lysozyme and Muc5AC secretion was measured at 24 hours by ELISA as described in the text. Secretion was enhanced by VIP and reduced by NPY. VIP also increased lysozyme and Muc7 secretion in the presence of LPS. Significance determined by 1-way ANOVA with Bonferroni posttest comparing all points at 48 hours. Data are mean ± SEM of 4 independent experiments using cultures from 4 different patients for each time point. **f)** CFU assays were carried out as described in the text and using airway surface liquid (ASL) washings after 24 hours (left bar graph) and 48 hours (right bar graph). Two clinical strains of *P. aeruginosa* were used. At both time points, VIP increased antimicrobial efficacy while NPY reduced it. Significance determined by 1-way ANOVA with Bonferroni posttest comparing all points at 48 hours. Data are mean ± SEM of 5 independent experiments using cultures from 5 different patients for each time point. Due to the increased antimicrobial capacity of culture secretion at 24 and 48 hours (vs 2 hours as shown in the main text), we altered the parameters of the assay to be able to measure CFUs. 40,000 and 80,000 CFUs were used as the starting inputs for 24 hour and 48 hour ASL experiments, respectively (vs 20,000 at 2 hours in the main text). ASL was also diluted 1:2 compared with the main text. These alterations allowed the CFUs obtained in this assay to be within a countable range.

SUPPLEMENTARY FIGURE S17

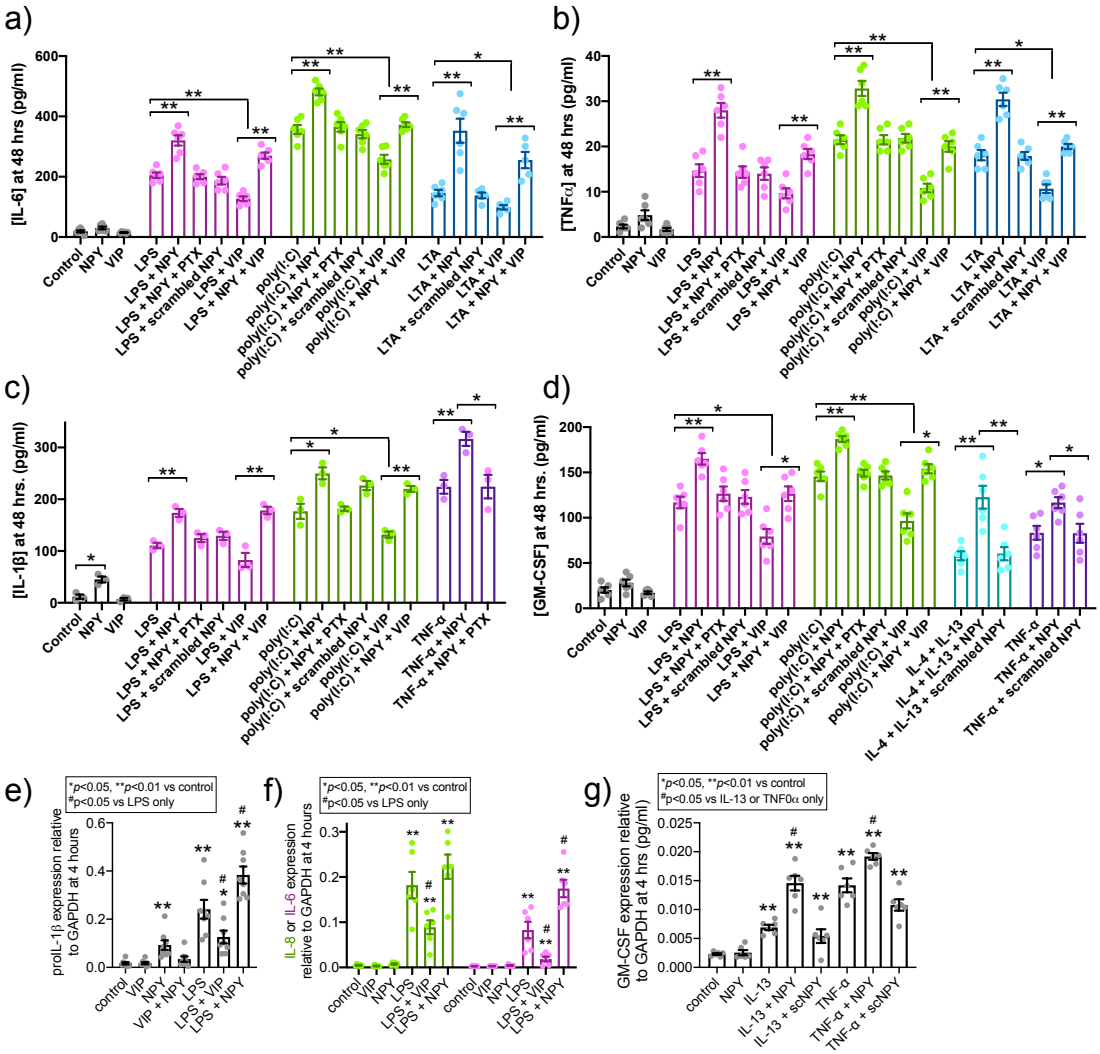

SUPPLEMENTARY FIGURE S17 Pro-inflammatory effects of NPY and anti-inflammatory effects fo VIP. Acinar cells from parotid and pancreatic exocrine glands can make and release cytokines [97-100]. Infection of isolated human tracheal submucosal gland cells with rhinovirus, which can activate TLR3 [101], increases IL-1α, IL-1β, IL-6, and IL-8 [102]. TLR4 is also expressed in pig tracheal acinar cells [103], and submucosal TLR4 levels may be elevated in CF [104]. Both VIP and NPY are immunomodulatory [105]. **a-d)** As described in the text, serous cell cultures were stimulated with TLR4 agonist LPS (1 μg/ml), TLR3 agonist poly(I:C) (5 μg/ml), TLR2 agonist LTA (1 μg/ml), TNFα (100 ng/ml) or a Th2 cocktail of IL-4 and IL-13 (20 ng/ml each; [106]) on the apical side only, with VIP (1 μM) and/or NPY (100 nM) or scrambled NPY (100 nM) on the basolateral side, or followed by collection of basolateral media and determination of IL-6 (*a*), TNFα (*b*), IL-1β (*c*), or GM-CSF (*d*) concentration by ELISA. In most cases, NPY potentiated inflammatory responses while VIP reduce them. The only cytokine affected by either VIP or NPY alone was IL-1β, which was increased by NPY. Bar graphs show individual experiments using at least 6 ALI cultures from at least 3 patients (2 ALIs per patient); Significance by 1-way ANOVA with Bonferroni posttest comparing secretion of each specific cytokine among bars within each color-matched group (LPS, poly(I:C), LTA, TNFα, or IL-4 and IL-13; **p*<0.05 and ***p*<0.01. These data agree with other studies showing VIP having anti-inflammatory or protective effects in parotid acini [105, 107-110] and NPY having pro-inflammatory effects in leukocytes [111]. GM-CSF and IL-1β that are important in allergic inflammation [112], neutrophil or eosinophil infiltration [113], and Th2 polarization [114]. Note that NPY itself increased IL-1β, and IL-1β polymorphisms may contribute to CF [115] or CRS [116]. It remains to be determined if these polymorphisms affect expression or secretion of IL-1β from gland acini. **e-g)** Cytokine mRNA was examined in serous ALIs stimulated as indicated for 4 hours. Isolated RNA was subject to reverse transcription quantitative PCR (qPCR) using TaqMan primers as indicated in the supplementary methods. Concentrations of agonists used are the same as in *a-d*. Significance by one-way ANOVA with Bonferroni posttest.

SUPPLEMENTARY FIGURE S18

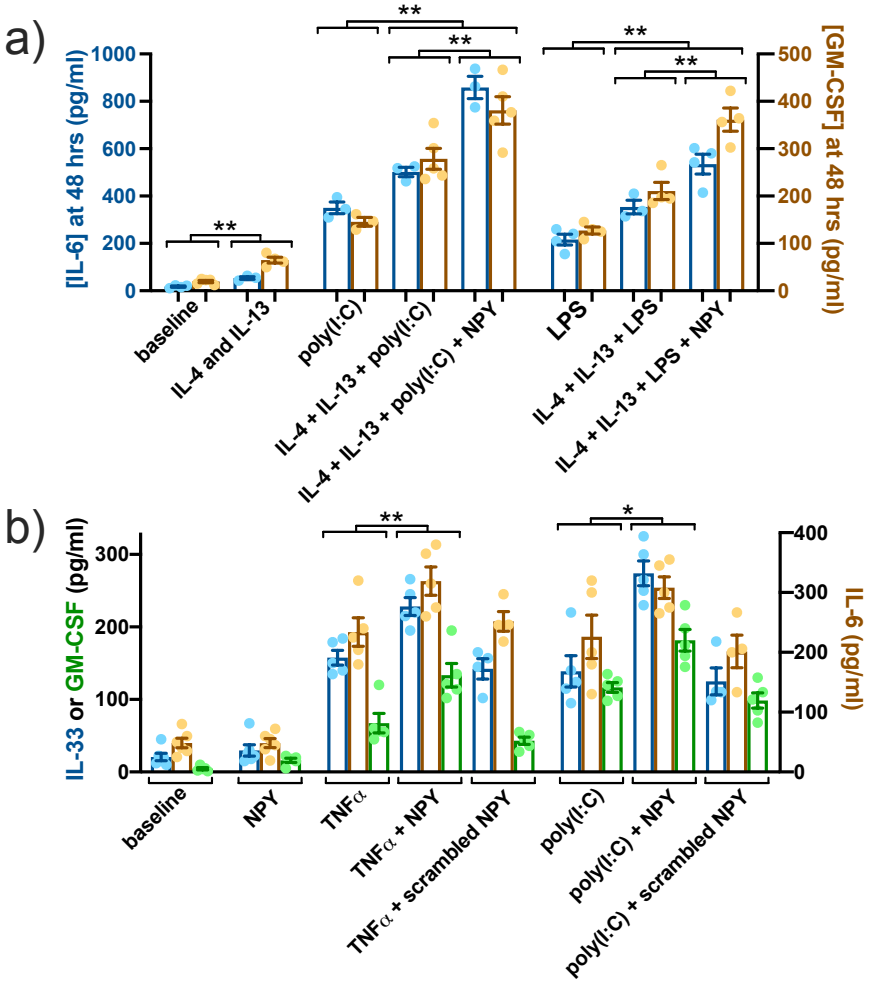

SUPPLEMENTARY FIGURE S18 Pro-inflammatory effects of NPY in cultured (A) and acutely isolated (B) airway gland serous cells. **a)** A strong Th2 environment by itself may increase other inflammatory responses in airway cells [117]. IL-6 and GM-CSF secretion was measured by ELISA using non-CF primary serous cell ALIs stimulated with a Th2 cytokine cocktail (IL-4 + IL-13) as well as TLR3 agonists poly(I:C) or TLR4 agonist (LPS) ± NPY for 48 hrs. IL-4 + IL-13 increased responses to poly(I:C) and LPS, and NPY had a further pro-inflammatory effect even in the presence of IL-4 and IL-13, suggesting that NPY can augment inflammatory responses even in the strong Th2 environment that accompanies many inflammatory airway diseases. Bar graphs show mean ± SEM from 3-5 individual experiments each using an ALI from a separate non-CF patients. Significance determined by 1-way ANOVA with Bonferroni posttest; *p<0.05 and **p<0.01. **b)** Isolated acinar cells were stimulated with TNFα or poly(I:C) ± NPY or scrambled NPY. NPY, but not scrambled NPY, increased secretion of IL-33, GM-CSF, and IL-6 (measured via ELISA) in response to both TNFα or poly(I:C) but had minimal effect on its own, supporting data from cultured cells. Bar graphs show mean ± SEM from 6 individual experiments using 2 ALIs each from 3 non-CF patients. Significance determined by 1-way ANOVA with Bonferroni posttest; *p<0.05 and **p<0.01.

SUPPLEMENTARY FIGURE S19

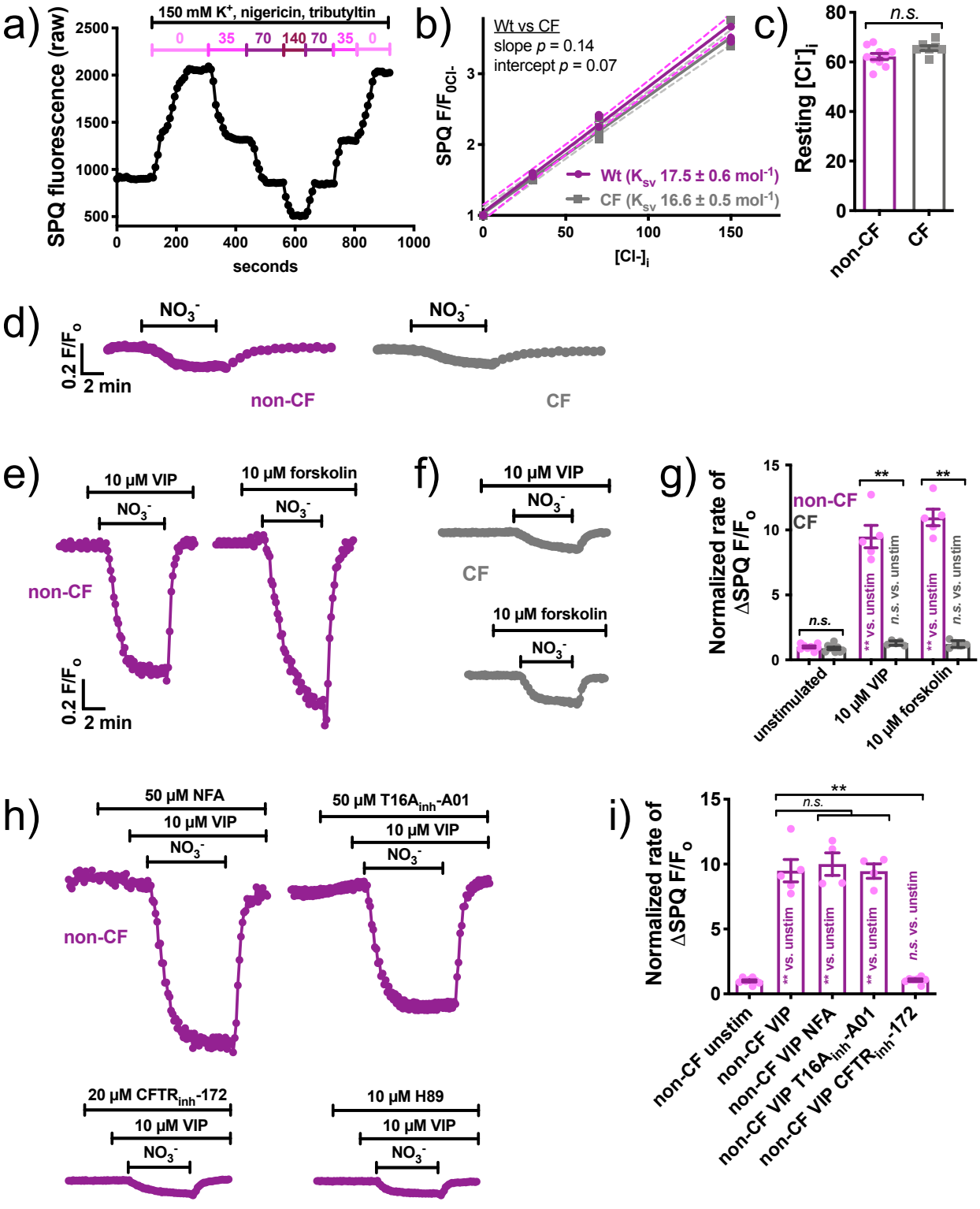

SUPPLEMENTARY FIGURE S19 Resting $[Cl^-]_i$ is not different in non-CF and CF serous cells, but CF serous cells lack VIP/cAMP-stimulated Cl^- permeability. Non-CF and CF serous cells were obtained and isolated from patient samples and loaded with Cl^- -sensitive dye SPQ as described in the supplementary methods and [3, 5, 6]. **a)** Representative trace of calibration of SPQ fluorescence at various $[Cl^-]_i$ values was carried out using high extracellular K^+ solution and H^+/K^+ exchanger nigericin and anion exchanger tributyltin. **b)** Stern-Volmer plot (as described [3]) showed Stern-Volmer constant (K_{SV}) values of ~17/mol for both genotypes and revealed similar resting $[Cl^-]_i$ **c)** Bar graph of resting $[Cl^-]_i$ (mean ± SEM) in non-CF and CF serous cells, which not significantly different by Student's *t* test. **d-g)** We examined Cl^- permeability using extracellular NO_3^- substitution with SPQ loaded cells. SPQ is quenched by Cl^- but not by NO_3^-, and Cl^- channels are nearly equally permeable to Cl^- and NO_3^-. NO_3^- substitution (0-Cl^-_o) revealed identical resting Cl^- permeabilities in non-CF and CF cells (*d, g*). However, when stimulated with VIP or forskolin, Cl^- permeability increased in non-CF but not CF cells (*e-g*). A downward deflection of traces reflects a decrease in $[Cl^-]_i$ (increase in SPQ F/F_o). Bar graph in *g* shows mean ± SEM; * and ** = p< 0.05 and 0.01, respectively (one-way ANOVA with Bonferroni posttest). All data points are independent experiments from 3-4 CF and 3-5 non CF patients (at least 2 independent acinar cell experiments per patient). These data show that cAMP-activated Cl^- permeability is absent in CF serous cells. **h-i)** In non-CF cells, increased Cl^- permeability in response to VIP was inhibited by $CFTR_{inh}172$ (CFTR inhibitor) or H89 (PKA inhibitor) but not by niflumic acid (NFA) or $T16A_{inh}$-A01 (Ca^{2+}-activated Cl^- channel inhibitors). Bar graph in I shows mean ± SEM; * and ** = *p*<0.05 and 0.01, respectively by one-way ANOVA with Bonferroni posttest. Thus, VIP-activated Cl^- permeability is cAMP-dependent and is blocked by CFTR inhibition.

SUPPLEMENTARY FIGURE S20

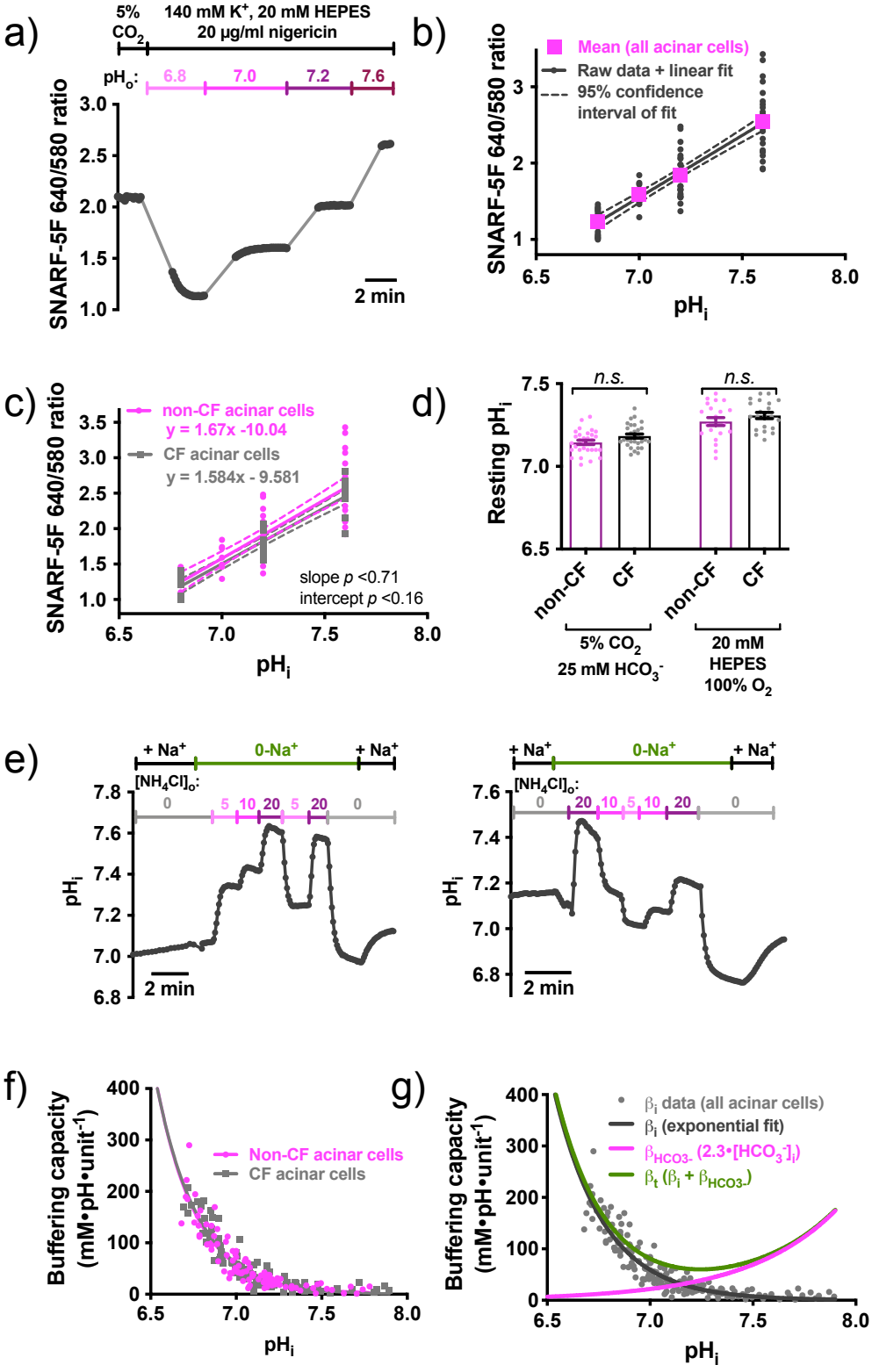

SUPPLEMENTARY FIGURE S20 Measurement of intracellular pH (pH_i) in serous cells from CF and non-CF patients. **a-c)** Non-CF and CF serous cells were loaded with the ratiometric intracellular pH (pH_i) indicator SNARF-5F. SNARF-5F fluorescence was calibrated using high K^+ solutions of known pH containing H^+/K^+ exchanger nigericin (as described in [4]). Example calibration shown in (a). *b* shows calibration of acinar cells of all genotypes and *c* shows CF vs non-CF cells. No differences were observed between CF and non-CF acinar cells (n = 3 patients each), allowing comparison of the SNARF responses in the two groups. **(D).** Resting pH_i was extrapolated from experiments in the presence or absence of HCO_3^-. No significant difference was observed in CF vs non-CF cells. Mean ± SEM; *n.s.* = not significantly different by one-way ANOVA with Bonferroni posttest. All data points are independent experiments from 3-4 CF and 3-5 non CF patients (at least 2 independent acinar cell experiments per patient). **e-g)** Intrinsic (HCO_3^--independent) pH_i buffering capacity (β_i) was measured using NH_3/NH_4 pulse method [described in [4, 35]) under 0-Na^+ conditions to reduce pH_i regulatory mechanisms. Because of marked variation in buffering capacity of various cell types due to size and organelle composition, β_i must be experimentally determined. Representative calibration experiments shown in (*e*). Pooled buffering capacity measurements were used to compare CF and non-CF acinar cells (*f*). No significant difference in β_i was observed between the two cells. This means pH_i changes similarly represent OH^- eq fluxes in the two groups; pH_i changes can thus be compared between the two groups. β_i was fit with an exponential decay curve (*g*) and combined with HCO_3^--dependent buffering (β_{HCO3-}) to calculate total buffering capacity (β_t) to convert pH_i changes to OH^- eq fluxes (not shown here). We measured pH_i changes in cells exposed to solutions of various $[NH_4Cl]_o$. Exposure of cells to a solution of NH_3-NH_4^+ leads to rapid entry of membrane-permeant NH_3 into the cell, causing pH_i alkalinization as H^+ is consumed as intracellular NH_3 converts to NH_4^+. This is followed by a slower acidification, likely NH_4^+ entry through K^+ channels or the Na^+/K^+ ATPase [34, 118]. Upon changing $[NH_3]_o$, the $[NH_4^+]_i$ can be calculated using Henderson-Hasselbach with $[NH_4^+]_i = [NH_3]_i \times 10^{pKa-pHi}$ with pKa of NH_3/NH_4^+ = 9.2 [35]. Solutions containing 0, 5, 10, and 20 mM $[NH_4Cl]_o$ contained 0, 0.6, 1.2, and 2.5 mM $[NH_3]_o$, respectively, at pH_o = 7.4. Buffering was calculated after an experimental change in $[NH_3]_o$ using the initial fast pH_i increase or decrease to estimate buffering power around the midpoint of the pH_i change $\Delta[NH_4^+]/\Delta pH_i$ (units of $mmol \bullet L^{-1}$ of acid or base equivalent required to change pH_i by one unit). Raw data points from experiments as in *e* were fit with an exponential decay function (*f*). No difference was observed between CF and non-CF acinar cells in β_i. Total buffering capacity (β_t; *g*) was calculated using all data points (both genotypes) and adding the β_i curve to β_{HCO3-} (2.3 x $[HCO_3^-]$, with $[HCO_3^-]_i$ calculated from Henderson Hasselbach with CO_2 clamped at 5%). See the supplementary methods and [4, 35] for more experimental information.

SUPPLEMENTARY FIGURE S21

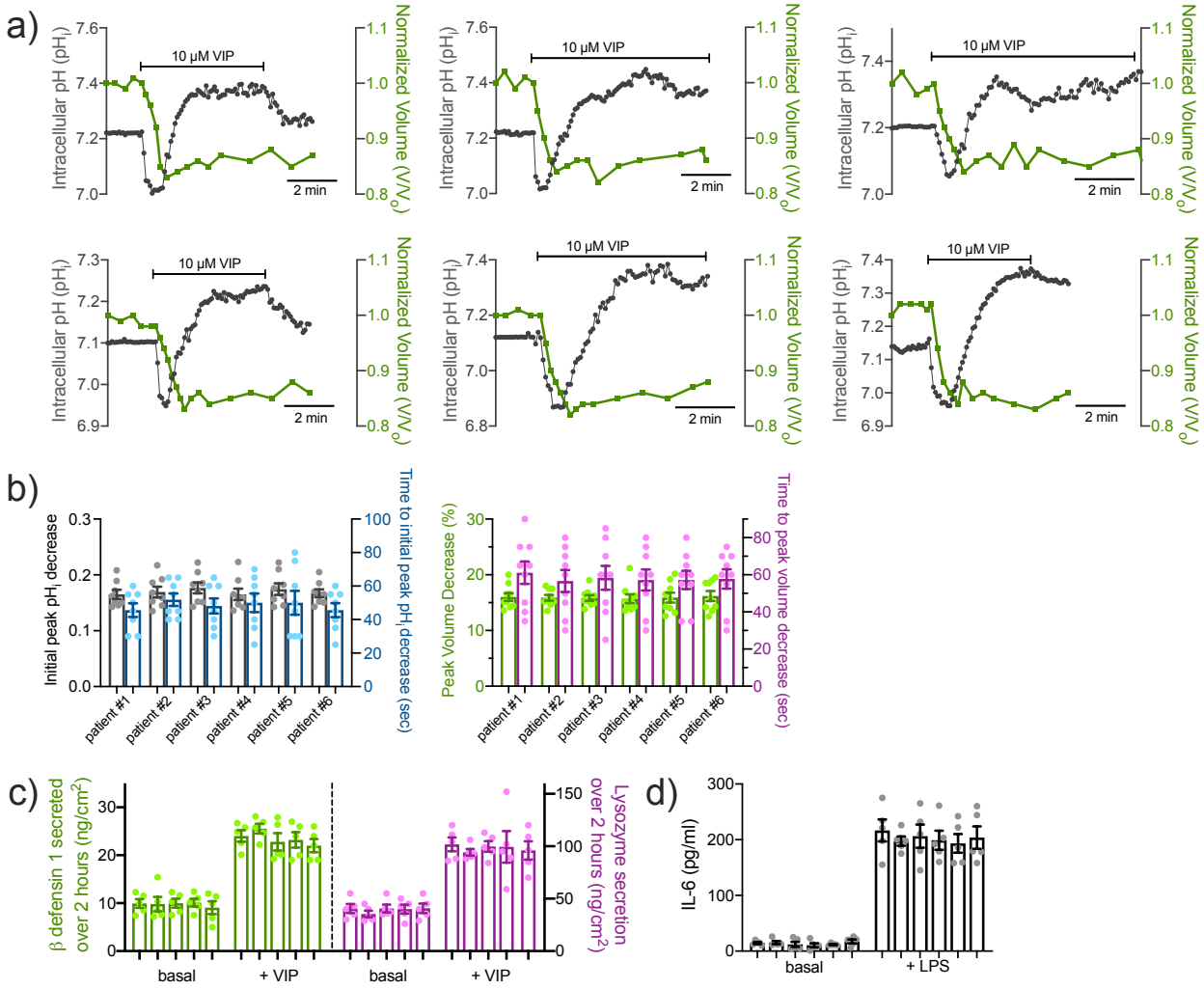

SUPPLEMENTARY FIGURE S21 Minimal patient-to-patient variability of responses in primary serous cells acutely isolated (*a-b*) and cultured at air-liquid interface (ALI) for 4 weeks (*c-d*). **a)** Representative responses to of intracellular pH_i (to track HCO_3^- secretion) and cell volume (to track Cl^- secretion) in primary ALIs from six different patients. **b)** quantification of responses from 9 independent acini imaged from each patient. No significant differences were observed by 1-way ANOVA. Note that resolution of time to peak shrinkage and time to peak pHi decrease values are limited by the 4 sec sampling frequency, used to limit phototoxicity and photobleaching during fluorescence live cell imaging experiments (as described in supplementary methods and [3, 5, 6, 30]). **c)** Quantification of β defensin 1 and lysozyme secretion in 4-week serous cell ALIs over 2 hours in unstimulated (basal) conditions and 10 μM VIP-stimulated conditions. No significant differences were observed by 1-way ANOVA. **d)** Quantification of IL-6 secretion at baseline (unstimulated) and after stimulation with 1 μg/ml LPS for 24 hours. No significant differences among patients were observed by 1-way ANOVA. Each bar graph in *c* and *d* shows mean ± SEM of 5 independent experiments from each patient. Together, these data suggest that culture-to-culture variability rather than patient-to-patient variability is the main variable factor in these types of experiments. In our experience with surface epithelial ALI cultures [10-18], we find that once primary cells are expanded and cultured for 3-6 weeks in defined media, secondary disease-related phenotypes are removed and cells reflect a "healthy" baseline state, with responses overwhelmingly dictated by genetics. This allows disease-relevant *in vitro* manipulations (treatment with IL-13, NPY, etc.) with comparison of unmanipulated cells from the same patient as "control."

SUPPLEMENTARY FIGURE S22

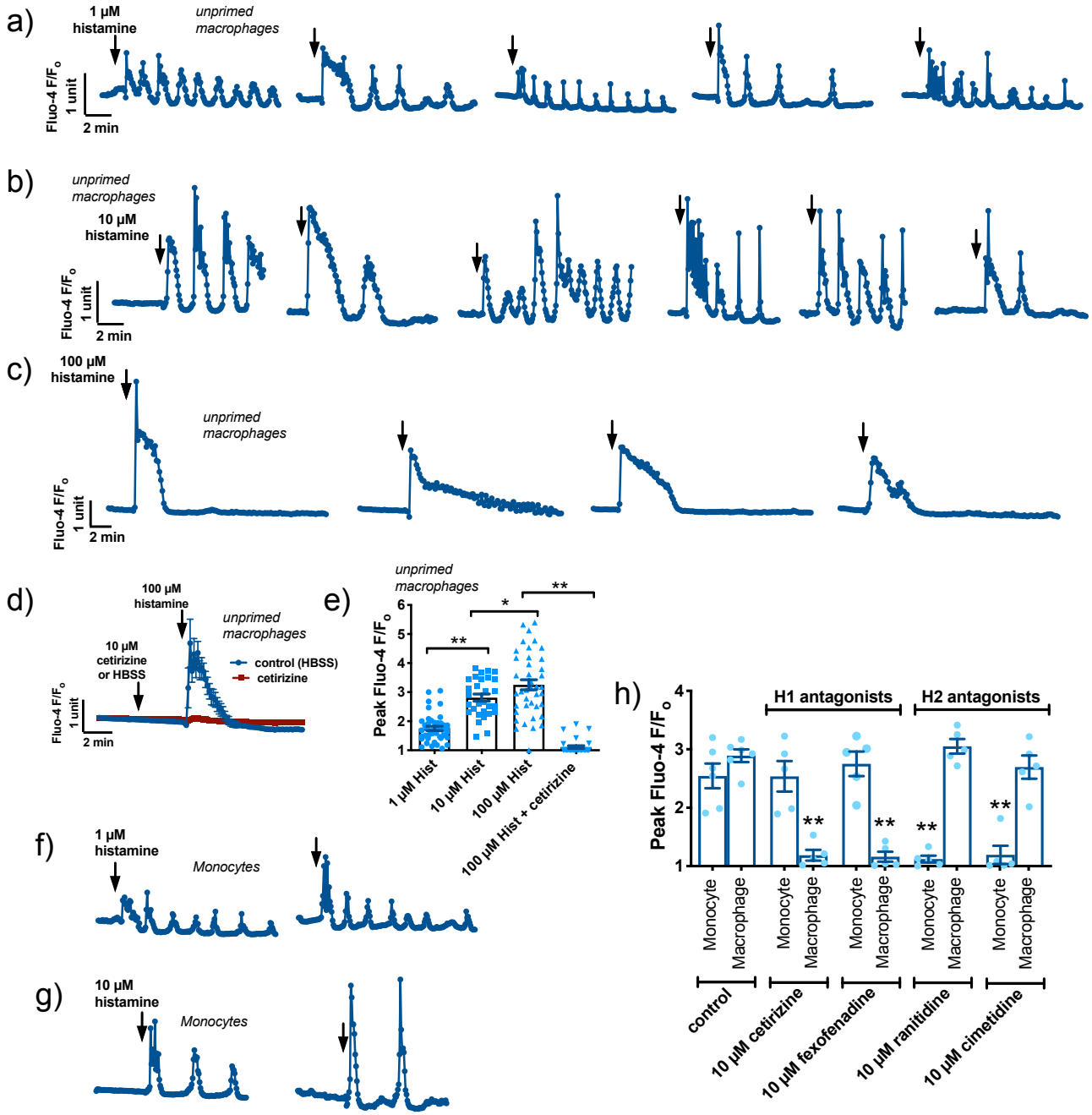

SUPPLEMENTARY FIGURE S22 Confirmation of Mϕ differentiation by functional H1 receptor expression. Differentiation of monocytes into MΦs is accompanied by switch of histamine receptor expression from H2 to H1 isoform [119-121]. **a-c)** Representative Ca^{2+} oscillations induced in individual Fluo-4 loaded MΦs by 1, 10 μM histamine as well as larger transients with 100 μM histamine in Mϕs differentiated for 10 days as indicated in the text. **d)** Average representative traces (~25 Mϕs) of response to 100 μM histamine in the absence (blue) or presence of 10 μM cetirizine (H1 antagonist). (E) Plot of responses from individual Mϕs from ≥3 independent experiments using Mϕs from ≥3 individuals. **f-g)** Representative Ca^{2+} oscillations from freshly isolated monocytes imaged on Cell-Tak-coated coverslips. **h)** Bar graph of individual experiments (n = 3-6 from ≥3 patients) showing inhibition of Ca^{2+} responses to 10 μM histamine by H1 antagonists cetirizine or fexofenadine in Mϕs and H2 antagonists ranitidine and cimetidine in monocytes. Bar graphs are mean ± SEM with significance determined by 1-way ANOVA with Bonferroni posttest; *p<0.05 and **p<0.01.

SUPPLEMENTARY REFERENCES

1. Tewson PH, Martinka S, Shaner NC, Hughes TE, Quinn AM. New DAG and cAMP Sensors Optimized for Live-Cell Assays in Automated Laboratories. *J Biomol Screen* 2016: 21(3): 298-305.

2. Kost TA, Kemp CW. Fundamentals of Baculovirus Expression and Applications. *Adv Exp Med Biol* 2016: 896: 187-197.

3. Lee RJ, Limberis MP, Hennessy MF, Wilson JM, Foskett JK. Optical imaging of Ca2+-evoked fluid secretion by murine nasal submucosal gland serous acinar cells. *J Physiol* 2007: 582(Pt 3): 1099-1124.

4. Lee RJ, Harlow JM, Limberis MP, Wilson JM, Foskett JK. HCO3(-) secretion by murine nasal submucosal gland serous acinar cells during Ca2+-stimulated fluid secretion. *J Gen Physiol* 2008: 132(1): 161-183.

5. Lee RJ, Foskett JK. Mechanisms of Ca2+-stimulated fluid secretion by porcine bronchial submucosal gland serous acinar cells. *Am J Physiol Lung Cell Mol Physiol* 2010: 298(2): 22.

6. Lee RJ, Foskett JK. cAMP-activated Ca2+ signaling is required for CFTR-mediated serous cell fluid secretion in porcine and human airways. *J Clin Invest* 2010: 120(9): 3137-3148.

7. Widdicombe JH, Wine JJ. Airway Gland Structure and Function. *Physiol Rev* 2015: 95(4): 1241-1319.

8. Lee RJ, Foskett JK. Ca2+ signaling and fluid secretion by secretory cells of the airway epithelium. *Cell Calcium* 2014: 55(6): 325-336.

9. Lee RJ, Foskett JK. Why mouse airway submucosal gland serous cells do not secrete fluid in response to cAMP stimulation. *J Biol Chem* 2012: 287(45): 38316-38326.

10. Lee RJ, Xiong G, Kofonow JM, Chen B, Lysenko A, Jiang P, Abraham V, Doghramji L, Adappa ND, Palmer JN, Kennedy DW, Beauchamp GK, Doulias P-T, Ischiropoulos H, Kreindler JL, Reed DR, Cohen NA. T2R38 taste receptor polymorphisms underlie susceptibility to upper respiratory infection. *J Clin Invest* 2012: 122(11): 4145-4159.

11. Lee RJ, Chen B, Doghramji L, Adappa ND, Palmer JN, Kennedy DW, Cohen NA. Vasoactive intestinal peptide regulates sinonasal mucociliary clearance and synergizes with histamine in stimulating sinonasal fluid secretion. *FASEB J* 2013: 27(12): 5094-5103.

12. Lee RJ, Kofonow JM, Rosen PL, Siebert AP, Chen B, Doghramji L, Xiong G, Adappa ND, Palmer JN, Kennedy DW, Kreindler JL, Margolskee RF, Cohen NA. Bitter and sweet taste receptors regulate human upper respiratory innate immunity. *J Clin Invest* 2014: 124(3): 1393-1405.

13. Lee RJ, Hariri BM, McMahon DB, Chen B, Doghramji L, Adappa ND, Palmer JN, Kennedy DW, Jiang P, Margolskee RF, Cohen NA. Bacterial d-amino acids suppress sinonasal innate immunity through sweet taste receptors in solitary chemosensory cells. *Sci Signal* 2017: 10(495).

14. McMahon DB, Workman AD, Kohanski MA, Carey RM, Freund JR, Hariri BM, Chen B, Doghramji LJ, Adappa ND, Palmer JN, Kennedy DW, Lee RJ. Protease-activated receptor 2 activates airway apical membrane chloride permeability and increases ciliary beating. *FASEB J* 2018: 32(1): 155-167.

15. Yan CH, Hahn S, McMahon D, Bonislawski D, Kennedy DW, Adappa ND, Palmer JN, Jiang P, Lee RJ, Cohen NA. Nitric oxide production is stimulated by bitter taste receptors ubiquitously expressed in the sinonasal cavity. *Am J Rhinol Allergy* 2017: 31(2): 85-92.

16. Lee RJ, Workman AD, Carey RM, Chen B, Rosen PL, Doghramji L, Adappa ND, Palmer JN, Kennedy DW, Cohen NA. Fungal Aflatoxins Reduce Respiratory Mucosal Ciliary Function. *Sci Rep* 2016: 6: 33221.

17. Zhao KQ, Cowan AT, Lee RJ, Goldstein N, Droguett K, Chen B, Zheng C, Villalon M, Palmer JN, Kreindler JL, Cohen NA. Molecular modulation of airway epithelial ciliary response to sneezing. *FASEB J* 2012: 26(8): 3178-3187.

18. Carey RM, Workman AD, Chen B, Adappa ND, Palmer JN, Kennedy DW, Lee RJ, Cohen NA. Staphylococcus aureus triggers nitric oxide production in human upper airway epithelium. *Int Forum Allergy Rhinol* 2015: 5(9): 808-813.

19. Hariri BM, McMahon DB, Chen B, Freund JR, Mansfield CJ, Doghramji LJ, Adappa ND, Palmer JN, Kennedy DW, Reed DR, Jiang P, Lee RJ. Flavones modulate respiratory epithelial innate immunity: anti-inflammatory effects and activation of the T2R14 receptor. *J Biol Chem* 2017: 292(20): 8484-8497.

20. Freund JR, Mansfield CJ, Doghramji LJ, Adappa ND, Palmer JN, Kennedy DW, Reed DR, Jiang P, Lee RJ. Activation of airway epithelial bitter taste receptors by Pseudomonas aeruginosa quinolones modulates calcium, cyclic-AMP, and nitric oxide signaling. *J Biol Chem* 2018: 293(25): 9824-9840.

21. Finkbeiner WE, Zlock LT, Mehdi I, Widdicombe JH. Cultures of human tracheal gland cells of mucous or serous phenotype. *In Vitro Cell Dev Biol Anim* 2010: 46(5): 450-456.

22. Fischer H, Illek B, Sachs L, Finkbeiner WE, Widdicombe JH. CFTR and calcium-activated chloride channels in primary cultures of human airway gland cells of serous or mucous phenotype. *Am J Physiol Lung Cell Mol Physiol* 2010: 299(4): L585-594.

23. Hariri BM, Payne SJ, Chen B, Mansfield C, Doghramji LJ, Adappa ND, Palmer JN, Kennedy DW, Niv MY, Lee RJ. In vitro effects of anthocyanidins on sinonasal epithelial nitric oxide production and bacterial physiology. *Am J Rhinol Allergy* 2016: 30(4): 261-268.

24. Tewson P, Westenberg M, Zhao Y, Campbell RE, Quinn AM, Hughes TE. Simultaneous detection of Ca2+ and diacylglycerol signaling in living cells. *PLoS One* 2012: 7(8): e42791.

25. Edelstein A, Amodaj N, Hoover K, Vale R, Stuurman N. Computer control of microscopes using microManager. *Curr Protoc Mol Biol* 2010: Chapter 14: Unit14 20.

26. Schwarz H, Villiger PM, von Kempis J, Lotz M. Neuropeptide Y is an inducible gene in the human immune system. *J Neuroimmunol* 1994: 51(1): 53-61.

27. Schindelin J, Arganda-Carreras I, Frise E, Kaynig V, Longair M, Pietzsch T, Preibisch S, Rueden C, Saalfeld S, Schmid B, Tinevez JY, White DJ, Hartenstein V, Eliceiri K, Tomancak P, Cardona A. Fiji: an open-source platform for biological-image analysis. *Nat Methods* 2012: 9(7): 676-682.

28. Foskett JK. Optical Imaging of Ion Transport in Single Living Cells. *Comments Mol Cell Biophys* 1993: 8(3): 115-135.

29. Foskett JK. Optical Studies of Ion and Water Transport in Single Living Cells. *In:* Grinstein S, and Foskett, J. K., ed. Noninvasive Techniques in Cell Biology. Wiley-Liss, Inc., New York, 1990; pp. 237-272.

30. Foskett JK. Simultaneous Nomarski and fluorescence imaging during video microscopy of cells. *Am J Physiol* 1988: 255(4 Pt 1): C566-571.

31. Verkman AS, Sellers MC, Chao AC, Leung T, Ketcham R. Synthesis and characterization of improved chloride-sensitive fluorescent indicators for biological applications. *Anal Biochem* 1989: 178(2): 355-361.

32. Foskett JK, Melvin JE. Activation of salivary secretion: coupling of cell volume and [Ca2+]i in single cells. *Science* 1989: 244(4912): 1582-1585.

33. Foskett JK. [Ca2+]i modulation of Cl- content controls cell volume in single salivary acinar cells during fluid secretion. *Am J Physiol* 1990: 259(6 Pt 1): C998-1004.

34. Roos A, Boron WF. Intracellular pH. *Physiol Rev* 1981: 61(2): 296-434.

35. Weintraub WH, Machen TE. pH regulation in hepatoma cells: roles for Na-H exchange, Cl-HCO3 exchange, and Na-HCO3 cotransport. *Am J Physiol* 1989: 257(3 Pt 1): G317-327.

36. Boron WF. Regulation of intracellular pH. *Adv Physiol Educ* 2004: 28(1-4): 160-179.

37. Renner EL, Lake JR, Persico M, Scharschmidt BF. Na+-H+ exchange activity in rat hepatocytes: role in regulation of intracellular pH. *Am J Physiol* 1989: 256(1 Pt 1): G44-52.

38. Kreindler JL, Bertrand CA, Lee RJ, Karasic T, Aujla S, Pilewski JM, Frizzell RA, Kolls JK. Interleukin-17A induces bicarbonate secretion in normal human bronchial epithelial cells. *Am J Physiol Lung Cell Mol Physiol* 2009: 296(2): L257-266.

39. Irokawa T, Krouse ME, Joo NS, Wu JV, Wine JJ. A "virtual gland" method for quantifying epithelial fluid secretion. *Am J Physiol Lung Cell Mol Physiol* 2004: 287(4): L784-793.

40. Hariri BM, McMahon DB, Chen B, Adappa ND, Palmer JN, Kennedy DW, Lee RJ. Plant flavones enhance antimicrobial activity of respiratory epithelial cell secretions against Pseudomonas aeruginosa. *PLoS One* 2017: 12(9): e0185203.

41. Alakomi HL, Skytta E, Saarela M, Mattila-Sandholm T, Latva-Kala K, Helander IM. Lactic acid permeabilizes gram-negative bacteria by disrupting the outer membrane. *Appl Environ Microbiol* 2000: 66(5): 2001-2005.

42. Johnson L, Mulcahy H, Kanevets U, Shi Y, Lewenza S. Surface-localized spermidine protects the Pseudomonas aeruginosa outer membrane from antibiotic treatment and oxidative stress. *J Bacteriol* 2012: 194(4): 813-826.

43. Wang J, Chou S, Xu L, Zhu X, Dong N, Shan A, Chen Z. High specific selectivity and Membrane-Active Mechanism of the synthetic centrosymmetric alpha-helical peptides with Gly-Gly pairs. *Sci Rep* 2015: 5: 15963.

44. Lv Y, Wang J, Gao H, Wang Z, Dong N, Ma Q, Shan A. Antimicrobial properties and membrane-active mechanism of a potential alpha-helical antimicrobial derived from cathelicidin PMAP-36. *PLoS One* 2014: 9(1): e86364.

45. Zhang Y, Reenstra WW, Chidekel A. Antibacterial activity of apical surface fluid from the human airway cell line Calu-3: pharmacologic alteration by corticosteroids and beta(2)-agonists. *Am J Respir Cell Mol Biol* 2001: 25(2): 196-202.

46. Widdicombe JH. Regulation of the depth and composition of airway surface liquid. *J Anat* 2002: 201(4): 313-318.

47. Seiler F, Hellberg J, Lepper PM, Kamyschnikow A, Herr C, Bischoff M, Langer F, Schafers HJ, Lammert F, Menger MD, Bals R, Beisswenger C. FOXO Transcription Factors Regulate Innate Immune Mechanisms in Respiratory Epithelial Cells. *Journal of Immunology* 2013: 190(4): 1603-1613.

48. Lund VJ, Mackay IS. Staging in rhinosinusitus. *Rhinology* 1993: 31(4): 183-184.

49. Lund VJ, Kennedy DW. Staging for rhinosinusitis. *Otolaryngol Head Neck Surg* 1997: 117(3 Pt 2): S35-40.

50. Quintanilla-Dieck L, Litvack JR, Mace JC, Smith TL. Comparison of disease-specific quality-of-life instruments in the assessment of chronic rhinosinusitis. *Int Forum Allergy Rhinol* 2012: 2(6): 437-443.

51. Ghandi M, Huang FW, Jane-Valbuena J, Kryukov GV, Lo CC, McDonald ER, 3rd, Barretina J, Gelfand ET, Bielski CM, Li H, Hu K, Andreev-Drakhlin AY, Kim J, Hess JM, Haas BJ, Aguet F, Weir BA, Rothberg MV, Paolella BR, Lawrence MS, Akbani R, Lu Y, Tiv HL, Gokhale PC, de Weck A, Mansour AA, Oh C, Shih J, Hadi K, Rosen Y, Bistline J, Venkatesan K, Reddy A, Sonkin D, Liu M, Lehar J, Korn JM, Porter DA, Jones MD, Golji J, Caponigro G, Taylor JE, Dunning CM, Creech AL, Warren AC, McFarland JM, Zamanighomi M, Kauffmann A, Stransky N, Imielinski M, Maruvka YE, Cherniack AD, Tsherniak A, Vazquez F, Jaffe JD, Lane AA, Weinstock DM, Johannessen CM, Morrissey MP, Stegmeier F, Schlegel R, Hahn WC, Getz G, Mills GB, Boehm JS, Golub TR, Garraway LA, Sellers WR. Next-generation characterization of the Cancer Cell Line Encyclopedia. *Nature* 2019: 569(7757): 503-508.

52. Shaul YD, Yuan B, Thiru P, Nutter-Upham A, McCallum S, Lanzkron C, Bell GW, Sabatini DM. MERAV: a tool for comparing gene expression across human tissues and cell types. *Nucleic Acids Res* 2016: 44(D1): D560-566.

53. Robertson MA, Foskett JK. Na+ transport pathways in secretory acinar cells: membrane cross talk mediated by [Cl-]i. *Am J Physiol* 1994: 267(1 Pt 1): C146-156.

54. Kreindler JL, Peters KW, Frizzell RA, Bridges RJ. Identification and membrane localization of electrogenic sodium bicarbonate cotransporters in Calu-3 cells. *Biochim Biophys Acta* 2006: 1762(7): 704-710.

55. Abdulnour-Nakhoul S, Nakhoul NL, Wheeler SA, Wang P, Swenson ER, Orlando RC. HCO3- secretion in the esophageal submucosal glands. *Am J Physiol Gastrointest Liver Physiol* 2005: 288(4): G736-744.

56. Namkoong E, Shin YH, Bae JS, Choi S, Kim M, Kim N, Hwang SM, Park K. Role of Sodium Bicarbonate Cotransporters in Intracellular pH Regulation and Their Regulatory Mechanisms in Human Submandibular Glands. *PLoS One* 2015: 10(9): e0138368.

57. Hong JH, Park S, Shcheynikov N, Muallem S. Mechanism and synergism in epithelial fluid and electrolyte secretion. *Pflugers Arch* 2013.

58. Gresz V, Kwon TH, Vorum H, Zelles T, Kurtz I, Steward MC, Aalkjaer C, Nielsen S. Immunolocalization of electroneutral Na(+)-HCO cotransporters in human and rat salivary glands. *Am J Physiol Gastrointest Liver Physiol* 2002: 283(2): G473-480.

59. Genovese M, Borrelli A, Venturini A, Guidone D, Caci E, Viscido G, Gambardella G, di Bernardo D, Scudieri P, Galietta LJV. TRPV4 and purinergic receptor signalling pathways are separately linked in airway epithelia to CFTR and TMEM16A chloride channels. *J Physiol* 2019.

60. Bernardinelli E, Costa R, Nofziger C, Paulmichl M, Dossena S. Effect of Known Inhibitors of Ion Transport on Pendrin (SLC26A4) Activity in a Human Kidney Cell Line. *Cellular Physiology and Biochemistry* 2016: 38(5): 1984-1998.

61. Namkung W, Phuan PW, Verkman AS. TMEM16A inhibitors reveal TMEM16A as a minor component of calcium-activated chloride channel conductance in airway and intestinal epithelial cells. *J Biol Chem* 2011: 286(3): 2365-2374.

62. Jang Y, Oh U. Anoctamin 1 in secretory epithelia. *Cell Calcium* 2014: 55(6): 355-361.

63. Hartzell C, Putzier I, Arreola J. Calcium-activated chloride channels. *Annu Rev Physiol* 2005: 67: 719-758.

64. Chiang L, Karvar S, Hamm-Alvarez SF. Direct imaging of RAB27B-enriched secretory vesicle biogenesis in lacrimal acinar cells reveals origins on a nascent vesicle budding site. *PLoS One* 2012: 7(2): e31789.

65. Xu S, Edman M, Kothawala MS, Sun G, Chiang L, Mircheff A, Zhu L, Okamoto C, Hamm-Alvarez S. A Rab11a-enriched subapical membrane compartment regulates a cytoskeleton-dependent transcytotic pathway in secretory epithelial cells of the lacrimal gland. *J Cell Sci* 2011: 124(Pt 20): 3503-3514.

66. Hsueh PY, Edman MC, Sun G, Shi P, Xu S, Lin YA, Cui H, Hamm-Alvarez SF, MacKay JA. Tear-mediated delivery of nanoparticles through transcytosis of the lacrimal gland. *J Control Release* 2015: 208: 2-13.

67. Rogers DF. The airway goblet cell. *Int J Biochem Cell Biol* 2003: 35(1): 1-6.

68. Stewart CE, Torr EE, Mohd Jamili NH, Bosquillon C, Sayers I. Evaluation of differentiated human bronchial epithelial cell culture systems for asthma research. *J Allergy (Cairo)* 2012: 2012: 943982.

69. Kreda SM, Okada SF, van Heusden CA, O'Neal W, Gabriel S, Abdullah L, Davis CW, Boucher RC, Lazarowski ER. Coordinated release of nucleotides and mucin from human airway epithelial Calu-3 cells. *J Physiol* 2007: 584(Pt 1): 245-259.

70. Zhou J, Perelman JM, Kolosov VP, Zhou X. Neutrophil elastase induces MUC5AC secretion via protease-activated receptor 2. *Mol Cell Biochem* 2013: 377(1-2): 75-85.

71. Rose MC, Piazza FM, Chen YA, Alimam MZ, Bautista MV, Letwin N, Rajput B. Model systems for investigating mucin gene expression in airway diseases. *J Aerosol Med* 2000: 13(3): 245-261.

72. Shao MX, Ueki IF, Nadel JA. Tumor necrosis factor alpha-converting enzyme mediates MUC5AC mucin expression in cultured human airway epithelial cells. *Proc Natl Acad Sci U S A* 2003: 100(20): 11618-11623.

73. Sikder MA, Lee HJ, Mia MZ, Park SH, Ryu J, Kim JH, Min SY, Hong JH, Seok JH, Lee CJ. Inhibition of TNF-alpha-induced MUC5AC mucin gene expression and production by wogonin through the inactivation of NF-kappaB signaling in airway epithelial cells. *Phytother Res* 2014: 28(1): 62-68.

74. Kim JO, Sikder MA, Lee HJ, Rahman M, Kim JH, Chang GT, Lee CJ. Phorbol ester or epidermal growth-factor-induced MUC5AC mucin gene expression and production from airway epithelial cells are inhibited by apigenin and wogonin. *Phytother Res* 2012: 26(12): 1784-1788.

75. Sharma P, Dudus L, Nielsen PA, Clausen H, Yankaskas JR, Hollingsworth MA, Engelhardt JF. MUC5B and MUC7 are differentially expressed in mucous and serous cells of submucosal glands in human bronchial airways. *Am J Respir Cell Mol Biol* 1998: 19(1): 30-37.

76. Martinez-Anton A, Debolos C, Garrido M, Roca-Ferrer J, Barranco C, Alobid I, Xaubet A, Picado C, Mullol J. Mucin genes have different expression patterns in healthy and diseased upper airway mucosa. *Clin Exp Allergy* 2006: 36(4): 448-457.

77. Berger JT, Voynow JA, Peters KW, Rose MC. Respiratory carcinoma cell lines. MUC genes and glycoconjugates. *Am J Respir Cell Mol Biol* 1999: 20(3): 500-510.

78. Ito Y, Iwashita J, Kudoh A, Kuramata C, Murata J. MUC5B mucin production is upregulated by fibronectin and laminin in human lung epithelial cells via the integrin and ERK dependent pathway. *Biosci Biotechnol Biochem* 2015: 79(11): 1794-1801.

79. Woo HJ, Yoo WJ, Bae CH, Song SY, Kim YW, Park SY, Kim YD. Leptin up-regulates MUC5B expression in human airway epithelial cells via mitogen-activated protein kinase pathway. *Exp Lung Res* 2010: 36(5): 262-269.

80. Bae CH, Kim JW, Ye SB, Song SY, Kim YW, Park SY, Kim YD. AMPK induces MUC5B expression via p38 MAPK in NCI-H292 airway epithelial cells. *Biochem Biophys Res Commun* 2011: 409(4): 669-674.

81. Vogel DY, Glim JE, Stavenuiter AW, Breur M, Heijnen P, Amor S, Dijkstra CD, Beelen RH. Human macrophage polarization in vitro: maturation and activation methods compared. *Immunobiology* 2014: 219(9): 695-703.

82. Murray PJ. Macrophage Polarization. *Annu Rev Physiol* 2017: 79: 541-566.

83. Wheway J, Herzog H, Mackay F. NPY and receptors in immune and inflammatory diseases. *Curr Top Med Chem* 2007: 7(17): 1743-1752.

84. Singer K, Morris DL, Oatmen KE, Wang T, DelProposto J, Mergian T, Cho KW, Lumeng CN. Neuropeptide Y is produced by adipose tissue macrophages and regulates obesity-induced inflammation. *PLoS One* 2013: 8(3): e57929.

85. Rasiah KK, Kench JG, Gardiner-Garden M, Biankin AV, Golovsky D, Brenner PC, Kooner R, O'Neill G F, Turner JJ, Delprado W, Lee CS, Brown DA, Breit SN, Grygiel JJ, Horvath LG, Stricker PD, Sutherland RL, Henshall SM. Aberrant neuropeptide Y and macrophage inhibitory cytokine-1 expression are early events in prostate cancer development and are associated with poor prognosis. *Cancer Epidemiol Biomarkers Prev* 2006: 15(4): 711-716.

86. Bedoui S, von Horsten S, Gebhardt T. A role for neuropeptide Y (NPY) in phagocytosis: implications for innate and adaptive immunity. *Peptides* 2007: 28(2): 373-376.

87. Kaushik KS, Stolhandske J, Shindell O, Smyth HD, Gordon VD. Tobramycin and bicarbonate synergise to kill planktonic Pseudomonas aeruginosa, but antagonise to promote biofilm survival. *NPJ Biofilms Microbiomes* 2016: 2: 16006.

88. Massip-Copiz MM, Santa-Coloma TA. Extracellular pH and lung infections in cystic fibrosis. *Eur J Cell Biol* 2018.

89. Newbrun E, Hoover CI, Ryder MI. Bactericidal action of bicarbonate ion on selected periodontal pathogenic microorganisms. *J Periodontol* 1984: 55(11): 658-667.

90. Dorschner RA, Lopez-Garcia B, Peschel A, Kraus D, Morikawa K, Nizet V, Gallo RL. The mammalian ionic environment dictates microbial susceptibility to antimicrobial defense peptides. *FASEB J* 2006: 20(1): 35-42.

91. Dobay O, Laub K, Stercz B, Keri A, Balazs B, Tothpal A, Kardos S, Jaikumpun P, Ruksakiet K, Quinton PM, Zsembery A. Bicarbonate Inhibits Bacterial Growth and Biofilm Formation of Prevalent Cystic Fibrosis Pathogens. *Front Microbiol* 2018: 9: 2245.

92. Workman AD, Carey RM, Kohanski MA, Kennedy DW, Palmer JN, Adappa ND, Cohen NA. Relative susceptibility of airway organisms to antimicrobial effects of nitric oxide. *Int Forum Allergy Rhinol* 2017: 7(8): 770-776.

93. Singh PK, Jia HP, Wiles K, Hesselberth J, Liu L, Conway BA, Greenberg EP, Valore EV, Welsh MJ, Ganz T, Tack BF, McCray PB, Jr. Production of beta-defensins by human airway epithelia. *Proc Natl Acad Sci U S A* 1998: 95(25): 14961-14966.

94. Lee SH, Kim JE, Lim HH, Lee HM, Choi JO. Antimicrobial defensin peptides of the human nasal mucosa. *Ann Otol Rhinol Laryngol* 2002: 111(2): 135-141.

95. Regenhard P, Goethe R, Phi-van L. Involvement of PKA, PKC, and Ca2+ in LPS-activated expression of the chicken lysozyme gene. *J Leukoc Biol* 2001: 69(4): 651-658.

96. Lefevre P, Melnik S, Wilson N, Riggs AD, Bonifer C. Developmentally regulated recruitment of transcription factors and chromatin modification activities to chicken lysozyme cis-regulatory elements in vivo. *Mol Cell Biol* 2003: 23(12): 4386-4400.

97. Dios ID. Inflammatory role of the acinar cells during acute pancreatitis. *World J Gastrointest Pharmacol Ther* 2010: 1(1): 15-20.

98. Yamakawa M, Weinstein R, Tsuji T, McBride J, Wong DT, Login GR. Age-related alterations in IL-1beta, TNF-alpha, and IL-6 concentrations in parotid acinar cells from BALB/c and non-obese diabetic mice. *J Histochem Cytochem* 2000: 48(8): 1033-1042.

99. Tanda N, Ohyama H, Yamakawa M, Ericsson M, Tsuji T, McBride J, Elovic A, Wong DT, Login GR. IL-1 beta and IL-6 in mouse parotid acinar cells: characterization of synthesis, storage, and release. *Am J Physiol* 1998: 274(1 Pt 1): G147-156.

100. Kempuraj D, Twait EC, Williard DE, Yuan Z, Meyerholz DK, Samuel I. The novel cytokine interleukin-33 activates acinar cell proinflammatory pathways and induces acute pancreatic inflammation in mice. *PLoS One* 2013: 8(2): e56866.

101. Zhu L, Lee PK, Lee WM, Zhao Y, Yu D, Chen Y. Rhinovirus-induced major airway mucin production involves a novel TLR3-EGFR-dependent pathway. *Am J Respir Cell Mol Biol* 2009: 40(5): 610-619.

102. Yamaya M, Sekizawa K, Suzuki T, Yamada N, Furukawa M, Ishizuka S, Nakayama K, Terajima M, Numazaki Y, Sasaki H. Infection of human respiratory submucosal glands with rhinovirus: effects on cytokine and ICAM-1 production. *Am J Physiol* 1999: 277(2): L362-371.

103. Murakami K, Tamada T, Nara M, Muramatsu S, Kikuchi T, Kanehira M, Maruyama Y, Ebina M, Nukiwa T. Toll-like receptor 4 potentiates Ca2+-dependent secretion of electrolytes from swine tracheal glands. *Am J Respir Cell Mol Biol* 2011: 45(5): 1101-1110.

104. Hauber HP, Tulic MK, Tsicopoulos A, Wallaert B, Olivenstein R, Daigneault P, Hamid Q. Toll-like receptors 4 and 2 expression in the bronchial mucosa of patients with cystic fibrosis. *Can Respir J* 2005: 12(1): 13-18.

105. Dimitrijevic M, Stanojevic S. The intriguing mission of neuropeptide Y in the immune system. *Amino Acids* 2013: 45(1): 41-53.

106. White SR, Martin LD, Stern R, Laxman B, Marroquin BA. Expression of IL-4/IL-13 receptors in differentiating human airway epithelial cells. *Am J Physiol Lung Cell Mol Physiol* 2010: 299(5): L681-693.

107. Hauk V, Calafat M, Larocca L, Fraccaroli L, Grasso E, Ramhorst R, Leiros CP. Vasoactive intestinal peptide/vasoactive intestinal peptide receptor relative expression in salivary glands as one endogenous modulator of acinar cell apoptosis in a murine model of Sjogren's syndrome. *Clin Exp Immunol* 2011: 166(3): 309-316.

108. Vanesa H, Mario C, Esteban G, Laura F, Daniel P, Rosanna R, Claudia PL. Neuroimmune aspects of Sjogren's syndrome: role of VIP/VPAC system in immune and salivary gland epithelial cell function. *Curr Pharm Des* 2014: 20(29): 4760-4765.

109. Calafat M, Larocca L, Roca V, Hauk V, Pregi N, Nesse A, Perez Leiros C. Vasoactive intestinal peptide inhibits TNF-alpha-induced apoptotic events in acinar cells from nonobese diabetic mice submandibular glands. *Arthritis Res Ther* 2009: 11(2): R53.

110. Li C, Zhu F, Wu B, Wang Y. Vasoactive Intestinal Peptide Protects Salivary Glands against Structural Injury and Secretory Dysfunction via IL-17A and AQP5 Regulation in a Model of Sjogren Syndrome. *Neuroimmunomodulation* 2017: 24(6): 300-309.

111. Chandrasekharan B, Nezami BG, Srinivasan S. Emerging neuropeptide targets in inflammation: NPY and VIP. *Am J Physiol Gastrointest Liver Physiol* 2013: 304(11): G949-957.

112. Roan F, Obata-Ninomiya K, Ziegler SF. Epithelial cell-derived cytokines: more than just signaling the alarm. *J Clin Invest* 2019: 129(4): 1441-1451.

113. Laan M, Prause O, Miyamoto M, Sjostrand M, Hytonen AM, Kaneko T, Lotvall J, Linden A. A role of GM-CSF in the accumulation of neutrophils in the airways caused by IL-17 and TNF-alpha. *Eur Respir J* 2003: 21(3): 387-393.

114. Ritz SA, Cundall MJ, Gajewska BU, Swirski FK, Wiley RE, Alvarez D, Coyle AJ, Stampfli MR, Jordana M. The lung cytokine microenvironment influences molecular events in the lymph nodes during Th1 and Th2 respiratory mucosal sensitization to antigen in vivo. *Clin Exp Immunol* 2004: 138(2): 213-220.

115. Levy H, Murphy A, Zou F, Gerard C, Klanderman B, Schuemann B, Lazarus R, Garcia KC, Celedon JC, Drumm M, Dahmer M, Quasney M, Schneck K, Reske M, Knowles MR, Pier GB, Lange C, Weiss ST. IL1B polymorphisms modulate cystic fibrosis lung disease. *Pediatr Pulmonol* 2009: 44(6): 580-593.

116. Erbek SS, Yurtcu E, Erbek S, Atac FB, Sahin FI, Cakmak O. Proinflammatory cytokine single nucleotide polymorphisms in nasal polyposis. *Arch Otolaryngol Head Neck Surg* 2007: 133(7): 705-709.

117. Herbert C, Do K, Chiu V, Garthwaite L, Chen Y, Young PM, Traini D, Kumar RK. Allergic environment enhances airway epithelial pro-inflammatory responses to rhinovirus infection. *Clin Sci (Lond)* 2017: 131(6): 499-509.

118. Boron WF, De Weer P. Intracellular pH transients in squid giant axons caused by CO2, NH3, and metabolic inhibitors. *J Gen Physiol* 1976: 67(1): 91-112.

119. Wang KY, Arima N, Higuchi S, Shimajiri S, Tanimoto A, Murata Y, Hamada T, Sasaguri Y. Switch of histamine receptor expression from H2 to H1 during differentiation of monocytes into macrophages. *FEBS Lett* 2000: 473(3): 345-348.

120. Ohno S, Shirai A, Ueda A, Igarashi T, Ishigatsubo Y, Tani K, Okubo T, Hikawa N, Kawakami T, Takenaka T. Increase in intracellular calcium induced by stimulating histamine H1 receptors in macrophage-like P388D1 cells. *Biochem Biophys Res Commun* 1991: 181(3): 1156-1163.

121. Marone G, Gentile M, Petraroli A, De Rosa N, Triggiani M. Histamine-induced activation of human lung macrophages. *Int Arch Allergy Immunol* 2001: 124(1-3): 249-252.